Rod Internal Pressure Quantification and Distribution Analysis Using FRAPCON

Fuel Cycle Research & Development

Prepared for
U.S. Department of Energy
Used Fuel Disposition Campaign

Ryan N. Bratton, Matt A. Jessee, and William A. Wieselquist
Oak Ridge National Laboratory

September 30, 2015
FCRD-UFD-2015-000636
Oak Ridge National Laboratory Report No.
ORNL/TM-2015/557

SUMMARY

This report documents work performed supporting the Department of Energy (DOE) Office of Nuclear Energy (NE) Fuel Cycle Technologies Used Fuel Disposition Campaign (UFDC) under work breakdown structure element 1.02.08.10, ST Analysis. In particular, this report fulfills the M4 milestone M4FT-15OR0810036, Quantify effects of power uncertainty on fuel assembly characteristics, within work package FT-15OR081003 – ST Analysis-ORNL. This research was also supported by the Consortium for Advanced Simulation of Light Water Reactors (http://www.casl.gov), an Energy Innovation Hub (http://www.energy.gov/hubs) for Modeling and Simulation of Nuclear Reactors under U.S. Department of Energy Contract No. DE-AC05-00OR22725.

The discharge rod internal pressure (RIP) and cladding hoop stress (CHS) distributions are quantified for Watts Bar Nuclear Unit 1 (WBN1) fuel rods by modeling core cycle design data, operation data (including modeling significant trips and downpowers), and as-built fuel enrichments and densities of each fuel rod in FRAPCON-3.5. A methodology is developed which tracks inter-cycle assembly movements and assembly batch fabrication information to build individual FRAPCON inputs for each evaluated WBN1 fuel rod. An alternate model for the amount of helium released from the zirconium diboride (ZrB_2) integral fuel burnable absorber (IFBA) layer is derived and applied to FRAPCON output data to quantify the RIP and CHS for these types of fuel rods. SCALE/Polaris is used to quantify fuel rod-specific spectral quantities and the amount of gaseous fission products produced in the fuel for use in FRAPCON inputs. Fuel rods with ZrB_2 IFBA layers (i.e., IFBA rods) are determined to have RIP predictions that are elevated when compared to fuel rod without IFBA layers (i.e., standard rods) despite the fact that IFBA rods often have reduced fill pressures and annular fuel pellets. The primary contributor to elevated RIP predictions at burnups less than and greater than 30 GWd/MTU is determined to be the total fuel rod void volume and the amount of released fission gas in the fuel rod, respectively. Cumulative distribution functions (CDFs) are prepared from the distribution of RIP and CHS predictions for all standard and IFBA rods. The provided CDFs allow for the determination of the portion of WBN1 fuel rods that exceed a specified RIP or CHS limit. Results are separated into IFBA and standard rods so that the two groups may be analyzed individually. FRAPCON results are provided in sufficient detail to enable the recalculation of the RIP while considering any desired plenum gas temperature, total void volume, or total amount of gas present in the void volume. A method to predict the CHS from a determined or assumed RIP is also proposed, which is based on the approximately linear relationship between the CHS and the RIP. Finally, improvements to the computational methodology of FRAPCON are proposed.

CONTENTS

SUMMARY iv

ACRONYMS xi

1. INTRODUCTION 1

2. METHODOLOGY 3
   - 2.1 Pre-Processing 4
   - 2.2 FRAPCON Input Generation 5
     - 2.2.1 Inter-cycle Assembly Movements 6
     - 2.2.2 Fuel Pellet Composition and Geometry 7
     - 2.2.3 Fuel Rod Geometry and Fabrication 9
     - 2.2.4 Irradiation and Operational History 10
     - 2.2.5 Fission Production of Gaseous Isotopes 11
     - 2.2.6 Fast Flux Factor 11
   - 2.3 Post-Processing 12

3. WATTS BAR NUCLEAR UNIT 1 15
   - 3.1 Summary Of Assumptions 16

4. RESULTS AND DISCUSSION 19
   - 4.1 Operating History 19
   - 4.2 FRAPCON Parameters 21
   - 4.3 Total Fuel Rod Void Volume 28
   - 4.4 Released Fission Gas 32
   - 4.5 IFBA Layer Helium Production 33
   - 4.6 Rod Internal Pressure 35
   - 4.7 Cladding Hoop Stress 37

5. ANALYSIS 41

6. CONCLUSIONS 46

FIGURES

Figure 2.1. A visualization of the operational history of a fuel rod. Data point colors correspond to the average fuel rod temperature. An inter-cycle down time of 50 days is assumed. 3

Figure 2.2. The axial power profile progression of a typical fuel rod across three consecutive fuel cycles. The shown axial power profiles consist of 53 axial nodes. 4

Figure 2.3. A simplified flowchart of the sequence of calculations of the FIG. 6

Figure 3.1. Radial orientation of WBN1 assemblies [12]. 15

Figure 3.2. Axial arrangement of WBN1 fuel rods [13]. 16

Figure 4.1. The distribution of discharge burnups for cycle 1 through cycle 10 fuel rods. 20

Figure 4.2. The distribution of peak rod-averaged fuel temperatures throughout the lifetimes of WBN1 cycle 1 through cycle 10 fuel rods. 20

Figure 4.3. The distribution of lifetime-averaged LHGRs of WBN1 cycle 1 through cycle 10 fuel rods. 21

Figure 4.4. Predictions of Γ calculated from SCALE/Polaris output data using equation 2.20. The fuel specific power was kept constant at 40 W/g and the initial enrichment was 3 wt.% U-235. 22

Figure 4.5. Predictions of Γ calculated from SCALE/Polaris output data using equation 2.20 with a constant specific power of 40 W/g evaluated at a fuel burnup of 60 GWd/MTU. 22

Figure 4.6. Predictions of Γ calculated from SCALE/Polaris output data using equation 2.20 with an initial enrichment of 3 wt.% U-235 evaluated at a fuel burnup of 60 GWd/MTU. 23

Figure 4.7. A visualization of trilinear interpolation where the desired prediction p lies between eight pre-calculated data points [15]. 24

Figure 4.8. The distribution of Γ predictions for WBN1 cycle 1 through cycle 10 fuel rods calculated from SCALE/Polaris output data using equation 2.20. 25

Figure 4.9. Predictions of F_{Fast} calculated from SCALE/Polaris output data using equation 2.23. The fuel specific power was kept constant at 40 W/g and the initial enrichment was 3 wt.% U-235. 26

Figure 4.10. Predictions of F_{Fast} calculated from SCALE/Polaris output data using equation 2.23. The fuel specific power and burnup correspond to 40 W/g and 60 GWd/MTU, respectively. 26

Figure 4.11. Predictions of F_{Fast} calculated from SCALE/Polaris output data using equation 2.23. The fuel specific power and initial enrichment correspond to 40 W/g and 3 wt.% U-235, respectively. 27

Figure 4.12. The distribution of predicted values for F_{Fast} calculated from SCALE/Polaris output data using equation 2.23. 27

Figure 4.13. The distribution of predicted values for total flux over the fast flux calculated from SCALE/Polaris output data. 28

Figure 4.14. Total void volume predictions for cycle 1 through cycle 10 fuel rods under vacuum drying conditions (P_{Ext}=133 Pa, T_F=400°C). 29

Figure 4.15. Total void volume predictions for cycle 1 through cycle 10 fuel rods under vacuum drying conditions (P_{Ext}=133 Pa, T_F=400°C). Colors correspond to the amount of data within each discharge burnup and void volume bin. 30

Figure 4.16. The distribution of total void volume predictions for cycle 1 through cycle 10 fuel rods under vacuum drying conditions (P_{Ext}=133 Pa, T_F=400°C). 30

Figure 4.17. Relative void volume predictions (V_f/V_i) for cycle 1 through cycle 10 fuel rods under vacuum drying conditions (P_{Ext}=133 Pa, T_F=400°C). Colors correspond to the amount of data within each discharge burnup and void volume bin. 31

Figure 4.18. The distribution of relative void volume predictions (V_f/V_i) for cycle 1 through cycle 10 fuel rods under vacuum drying conditions (P_{Ext}=133 Pa, T_F=400°C). 31

Figure 4.19. Released fission gas predictions for cycle 1 through cycle 10 fuel rods of WBN1. 32

Figure 4.20. Released fission gas predictions for cycle 1 through cycle 10 fuel rods of WBN1. Colors correspond to the amount of data within each discharge burnup and released fission gas bin. 33

Figure 4.21. The distribution of released fission gas predictions for cycle 1 through cycle 10 fuel rods of WBN1. 33

Figure 4.22. The B-10 utilization factor of each ZrB_2 IFBA layer vs. discharge burnup for cycle 1 through cycle 10 fuel rods of WBN1, calculated using equation 2.31. 34

Figure 4.23. The distribution of helium released from ZrB_2 IFBA layers for cycle 1 through cycle 10 IFBA rods of WBN1, calculated from Polaris output data using equation 2.31. 35

Figure 4.24. Rod internal pressure predictions for cycle 1 through cycle 10 fuel rods under vacuum drying conditions (P_{Ext}=133 Pa, T_F=400°C). 36

Figure 4.25. Rod internal pressure predictions for cycle 1 through cycle 10 fuel rods under vacuum drying conditions (P_{Ext}=133 Pa, T_F=400°C). Colors correspond to the amount of data within each discharge burnup and RIP bin. 36

Figure 4.26. The distribution of rod internal pressures for cycle 1 through cycle 10 fuel rods under vacuum drying conditions (P_{Ext}=133 Pa, T_F=400°C). 37

Figure 4.27. Cladding hoop stress factor predictions for cycle 1 through cycle 10 fuel rods under vacuum drying conditions (P_{Ext}=133 Pa, T_F=400°C). Colors correspond to the amount of data within each discharge burnup and cladding hoop stress factor bin. 38

Figure 4.28. The distribution of cladding hoop stress factor predictions for cycle 1 through cycle 10 fuel rods under vacuum drying conditions (P_{Ext}=133 Pa, T_F=400°C). 38

Figure 4.29. Cladding hoop stress predictions for cycle 1 through cycle 10 fuel rods under vacuum drying conditions (P_{Ext}=133 Pa, T_F=400°C). 39

Figure 4.30. Cladding hoop stress predictions for cycle 1 through cycle 10 fuel rods under vacuum drying conditions (P_{Ext}=133 Pa, T_F=400°C). Colors correspond to the amount of data within each discharge burnup and cladding hoop stress bin. 40

Figure 4.31. The distribution of cladding hoop stress predictions for cycle 1 through cycle 10 fuel rods at vacuum drying conditions (P_{Ext}=133 Pa, T_F=400°C). 40

Figure 5.1. The rod internal pressure cumulative distribution function for cycle 1 through cycle 10 standard rods under vacuum drying conditions at various rod-averaged plenum gas temperatures. 43

Figure 5.2. The rod internal pressure cumulative distribution function for cycle 1 through cycle 10 IFBA rods under vacuum drying conditions at various rod-averaged plenum gas temperatures. 44

Figure 5.3. The cladding hoop stress cumulative distribution function for cycle 1 through cycle 10 standard rods under vacuum drying conditions at various rod-averaged plenum gas temperatures. 44

Figure 5.4. The cladding hoop stress cumulative distribution function for cycle 1 through cycle 10 IFBA rods under vacuum drying conditions at various rod-averaged plenum gas temperatures. 45

ACRONYMS

BOC	beginning-of-cycle
BOL	beginning-of-life
CASL	Consortium for Advanced Simulation of Light Water Reactors
CDF	cumulative distribution function
CHS	cladding hoop stress
DSC	dry storage cask
EFPD	effective full-power days
EOC	end-of-cycle
FGR	fission gas release
FIG	FRAPCON input generator
GT	guide tube
GWd/MTU	gigawatt days per metric ton uranium
HDF	hierarchical data format
IFBA	integral fuel burnable absorber
IT	instrument tube
LHGR	linear heat generation rate
MCNP	Monte Carlo N-Particle
MTU	metric ton uranium
NPP	Nuclear Power Plant
NRC	Nuclear Regulatory Commission
PNNL	Pacific Northwest National Laboratory
PWR	pressurized water reactor
RCCA	rod cluster control assembly
RIP	rod internal pressure
TVA	Tennessee Valley Authority
SNF	spent nuclear fuel
UOX	uranium oxide
US	United States
WBN1	Watts Bar Nuclear Unit 1
wt.%	weight percent
ZrB_2	zirconium diboride

USED FUEL DISPOSITION ROD INTERNAL PRESSURE QUANTIFICATION AND DISTRIBUTION ANALYSIS USING FRAPCON

1. INTRODUCTION

Dry storage of spent nuclear fuel (SNF) has been in practice since the late 1980s. An event of chief concern to SNF management is a cladding wall failure where radioactive isotopes accumulated in the fuel void volume are allowed to escape into the storage container. Damaged SNF adds to the complexity of SNF management, therefore, it is advantageous to predict under what conditions these failures are likely to occur for SNF. The cladding stress serves as a useful metric for this purpose since the likelihood of a cladding failure is proportional to the cladding stress. In addition to the fuel burnup, the irradiation history of SNF (i.e., how much power the fuel produced as a function of time while it was in a nuclear reactor core) may also need to be considered when preparing SNF for storage because fuel temperatures during irradiation have an effect on the amount of fission gas and internal pressure of the fuel rod [2,3], which are important parameters to consider regarding cladding mechanical performance for storage and subsequent transportation. The significance of detailed time-dependent data, which are often not available, imposes an added challenge on high-BU SNF modeling. Previous analyses of high burnup SNF commonly only consider an assembly-averaged irradiation history, the results of which have limited applicability since the irradiation histories of the fuel rods are not being modeled explicitly. Modeling fuel rods in high or full fidelity is meaningful in order to predict fuel rod stress profiles over its lifetime.

A scenario of SNF handling where the cladding stresses have been observed to be elevated is the vacuum drying process of a dry storage canister (DSC) [4] where the temperature of the DSC increases to a maximum temperature of 400°C [5] and is evacuated of the contained water and backfilled with helium. Since undamaged SNF rods are sealed systems, the rod internal pressure (RIP) of the fuel rod and the low pressure of the DSC interior during vacuum drying impose a stress gradient across the fuel cladding. The stress gradient across the fuel cladding and the elevated temperatures allow for the dissolution and subsequent precipitation and reorientation of zirconium hydrides present in the cladding. During the cooling of the DSC, hydrides can precipitate in a radial orientation. Radial hydrides decrease cladding ductility [6] and, when present at a crack tip, can contribute to cladding crack elongation, potentially causing a breach and subsequent leakage of fission products.

The quantification of distribution of the RIP and the cladding stress for every fuel rod of a well-defined reactor system provides insight into the portion of fuel rods that could potentially experience significant hydride reorientation or a cladding failure during the vacuum drying process. Further, any fuel rods that are identified as in danger of a cladding failure could have their operational histories and manufacturing information analyzed to determine the cause of its elevated cladding stress or RIP. The Consortium for Advanced Simulation of Light Water Reactors (CASL) is developing advanced analysis tools that focus on high- fidelity modeling of a nuclear reactor system at the fuel rod level. The analyses performed as a part of the CASL project provide the necessary operational history data to perform the analyses of interest in the current work.

This report will first describe the methodology that was developed and utilized in order to quantify the RIP and cladding stresses of fuel rods for a well-defined reactor system. Once the methodology for the high-fidelity fuel rod modeling has been established, the chosen reactor system will be introduced along with the data that are available for the system and what assumptions must be made to perform the proposed analysis. RIP and cladding stress predictions will be shown and analyzed along with other pertinent output quantities. Finally, the implications of the results will be discussed and conclusions will be drawn and potential future work will be discussed.

2. METHODOLOGY

FRAPCON-3.5 has been chosen as the steady-state fuel performance code for this analysis, as it is the licensing tool of the Nuclear Regulatory Commission (NRC) and developed by Pacific Northwest National Laboratory (PNNL). FRAPCON can model fuel rods with detailed operational histories, including axial power profiles, to produce discharge RIP and cladding hoop stress (CHS) predictions. A methodology has been developed to facilitate the process of generating detailed FRAPCON inputs, which contain fuel rod fabrication and operational history data for each unique fuel rod of the reactor system. A visualization of the operating history data that are required for a single fuel rod is shown in Figure 2.1 as the rod-averaged linear heat generation rate (LHGR) as a function of the irradiation time in effective full power days (EFPD). Data points in Figure 2.1 are colored with respect to the average fuel temperature. Throughout the three fuel cycles shown in Figure 2.1 the axial power profile of the fuel rod is changing, a behavior that can be modeled in each FRAPCON input. An example of the evolution of the axial power profile as a function of irradiation time is shown in Figure 2.2, where the beginning-of-cycle (BOC) axial power profile is shown for each of the three fuel cycles displayed in Figure 2.1. As is shown in Figure 2.2, the axial power profile of a fresh fuel rod has an approximate cosine shape. As the fuel rod is irradiated, the axial center of the fuel is depleted at a rate that is higher than the other axial location of the fuel due to the increased power in that region. The fast depletion of the center of the fuel rod suppresses the power production in that region for future cycles, which is what causes the "double hump" axial power profile that is observed at the beginning of fuel cycles 2 and 3.

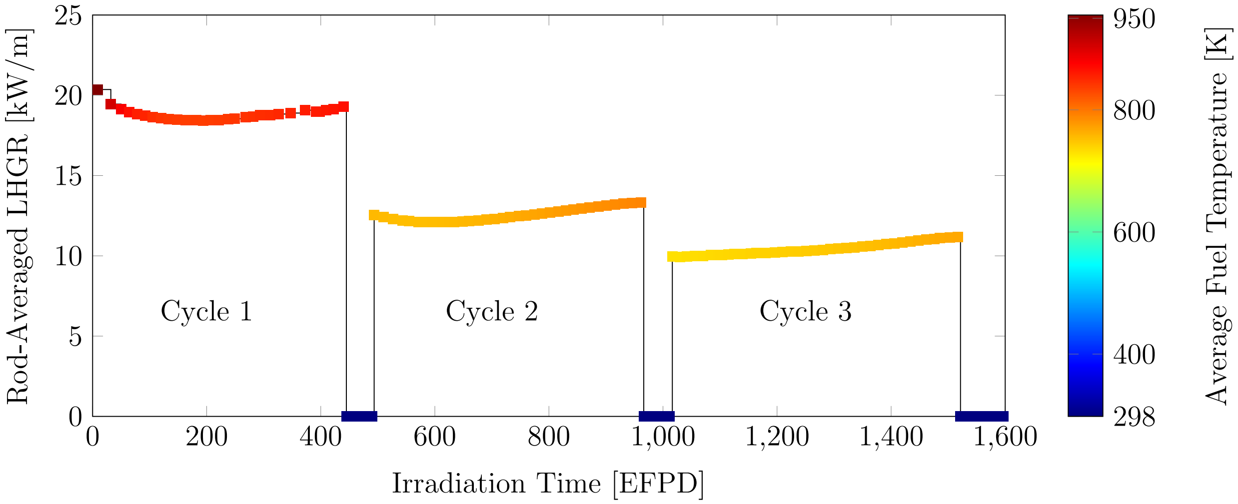

Figure 2.1. A visualization of the operational history of a fuel rod. Data point colors correspond to the average fuel rod temperature. An inter-cycle down time of 50 days is assumed.

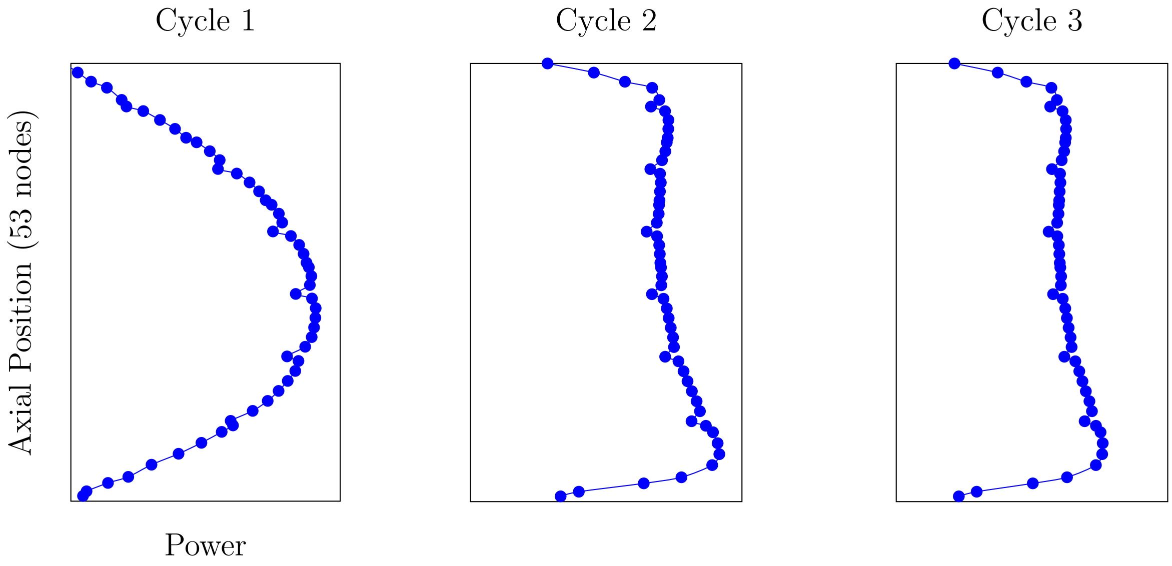

Figure 2.2. The axial power profile progression of a typical fuel rod across three consecutive fuel cycles. The shown axial power profiles consist of 53 axial nodes.

Detailed fuel rod-specific irradiation histories across an entire core are provided as output from core simulators. Often, the fuel rod-specific operational history data are stored as hierarchical data format (HDF) files [7], which can be accessed by Python scripts. The process of producing distributions of SNF parameters from the HDF files can be separated into three phases: pre-processing, FRAPCON input generation, and post-processing. The pre-processing phase involves refining the large amounts of pin-level operational history data that are stored in HDF files by calculating quantities that are utilized directly in the FRAPCON inputs and storing them in files that can be quickly accessed while the FRAPCON inputs are being generated. The next phase is the generation and execution of the FRAPCON inputs, which utilizes assembly batch information, inter-cycle assembly movements, core-level operational history data, and the fuel rod-level operational history data prepared in the pre-processing phase to generate a unique input for each fuel rod of chosen reactor system. The post-processing phase is where the FRAPCON results of each fuel rod are extracted to calculate the output parameters of interest. In general, the results from the FRAPCON outputs can be utilized directly, but additional steps are necessary to quantify the RIP and CHS for IFBA rods.

2.1 Pre-Processing

The purpose of the pre-processing phase is to extract the voluminous amount of data from the HDF files. Reading data from the HDF files is not performed during the generation of FRAPCON inputs because it is a time-consuming process, utilizing a few seconds to access data from one statepoint (or time step). A few seconds would not be significant for most analyses but when multiplied over the number of time steps (about 35) and the number of unique pins per cycle (over 5,000), this operation would take days to complete.

The pre-processing procedure includes four distinct accesses of HDF files per cycle to extract i) the time intervals of the core power history (in effective full-power days, EFPD), ii) the coolant inlet temperature for each time interval, iii) the beginning-of-cycle (BOC) and end-of-cycle (EOC) burnups for each fuel pin and iv) the axial power history of each fuel rod for each time step. Steps i) and ii) are simple processes that generate text files for each fuel cycle that will be read directly during FRAPCON input generation. The burnup files generated in step iii) allow the fuel rod locations between cycles to be verified by confirming that the EOC burnup from the previous cycle matches what is given for the BOC burnup for the next cycle. The files generated by step iv) contain the axial power profiles of each fuel rod at a particular time step and fuel cycle and are normalized by the pin peaking factor (P_{Pin}) for that particular fuel rod:

$$q' = \bar{q}' P_{Pin}, \tag{2.1}$$

where q' is the axially-averaged linear heat generation rate (LHGR) of the fuel rod and $\bar{q}'$ is the average pin LHGR of the core for that cycle and can be written as

$$\bar{q}' = \frac{\bar{P}_{Core}}{N_{Pins} L_{Fuel}}, \tag{2.2}$$

where $\bar{P}_{Core}$ is the cycle-averaged power of the core, N_{Pins} is the total number of fuel pins, and L_{Fuel} is the active fuel length of the fuel rod. The pin peaking factor (P_{Pin}) can be quantified as the volume-averaged sum of the axial power profile:

$$P_{Pin} = \sum_{n=1}^{N} \frac{z_n - z_{n-1}}{L_{Fuel}} q'_n, \tag{2.3}$$

where N is the number of axial nodes, z_n is the axial position and q'_n is the local power of the nth axial node. Axial power profiles are automatically normalized to unity in FRAPCON so P_{Pin} must be quantified for each time step of each fuel rod in order to calculate q'. Utilizing equations 2.1, 2.2, and 2.3, q' is predicted for every fuel rod at each time step and stored in a text file for access during the generation of the FRAPCON inputs.

2.2 FRAPCON Input Generation

At the conclusion of the pre-processing step, the operational history of each fuel pin of each cycle of the chosen reactor system has been extracted from the HDF files and recalculated as values that can be directly utilized in FRAPCON inputs. At this point, however, a multitude of other values must be calculated before a FRAPCON input can be generated for a fuel pin. In addition, each fuel pin must have its inter-cycle movements correctly tracked in order to generate a representative lifetime irradiation history for each fuel rod. These operations are performed by the FRAPCON input generator (FIG), which is written entirely in BASH. A simplified flow chart of the FIG is shown in Figure 2.2. This section will first outline how fuel rods are tracked during inter-cycle movements and then describe the calculation of each necessary FRAPCON parameter as performed by the FIG.

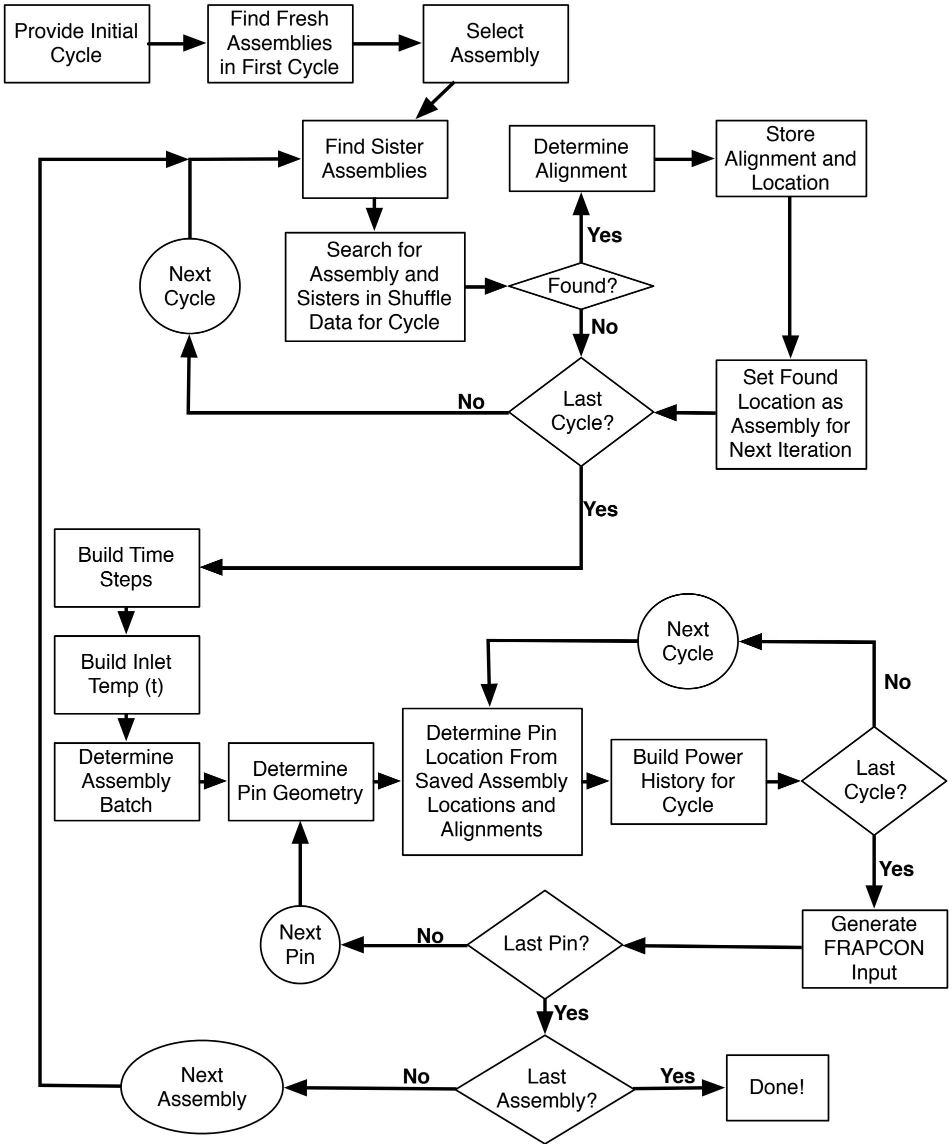

Figure 2.3. A simplified flowchart of the sequence of calculations of the FIG.

2.2.1 Inter-cycle Assembly Movements

The modeling of the movement of each assembly between fuel cycles is essential in order to obtain a representative power history of a fuel rod. In quarter-rotational symmetry, whenever an assembly is moved out of the quadrant that is being modeled, another rotationally-symmetric sister assembly is placed into the quadrant of interest. This can be replicated by taking the original assembly and “rotating" it so that it corresponds to its sister assembly and then placing it in the sister assembly's location for the subsequent cycle. The assembly rotation is performed only virtually and is a convenience of quarter-rotational core symmetry - in reality fuel assemblies are not rotated and always face the same direction for every cycle. Core simulators often consider some degree of rotational symmetry in the core in order to decrease the computational resources that are required for the simulation. This assumption can often be made with minimal error if the design of the core is symmetric and if assemblies are moved in rotationally-symmetric groups, which are referred to as sister assemblies. This operation is outlined in the upper half of the flowchart shown in Figure 2.3. In the FIG, assembly movements are verified by comparing the exiting and entering exposures of each fuel pin of each cycle since it is a convenient way to verify that the pins of two different cycles are identical. It is important to note that the exiting and entering fuel cycles need not be consecutive so if an assembly is not found in the subsequent cycle, the remaining cycles should also be searched.

2.2.2 Fuel Pellet Composition and Geometry

The compositional detail of the fuel material in FRAPCON is limited to a rod-averaged U-235 enrichment and density. The fuel region of modern pressurized water reactor (PWR) fuel is typically composed of fuel pellets and top and bottom fuel blankets. Each of these regions (i.e., pellet and blanket) can have unique enrichments and densities so a volume-weighted average of these values must be calculated for use in FRAPCON. A volume-weighted average is necessary since the fuel blankets may be annular. Fuel enrichments and densities are provided to FRAPCON in the units of atom percent U-235 and percent theoretical UO_2 density (10.96 g/cm^3), respectively, so additional calculations are required to convert the values provided by the reactor system manufacturer into what is utilized in FRAPCON.

The fuel enrichments for the pellet and blanket regions (provided in weight percent (wt.%) U-235) may be used to calculate the atom percent of U-235 of the fuel region (γ) by

$$\gamma = \frac{\varepsilon_{U-235}}{M_{U-235}} \frac{1}{\frac{\varepsilon_{U-234}}{M_{U-234}} + \frac{\varepsilon_{U-235}}{M_{U-235}} + \frac{\varepsilon_{U-236}}{M_{U-236}} + \frac{\varepsilon_{U-238}}{M_{U-238}}}, \tag{2.4}$$

where M_{U-234}, M_{U-235}, M_{U-236}, and M_{U-238} correspond to the molecular masses of U-234, U-235, U-236, and U-238, respectively and ε_{U-234}, ε_{U-235}, ε_{U-236}, and ε_{U-238}correspond to the weight-percent enrichments of U-234, U-235, U-236, and U-238, respectively. The volume-averaged enrichment that will be provided to FRAPCON can be calculated from the atom percent of U-235 for the fuel pellet and blanket regions (Pellet and Blanket, respectively):

$$\gamma = \gamma_{Pellet} \frac{V_{Pellet}}{V_{Pellet} + V_{Blanket}} + \gamma_{Blanket} \frac{V_{Blanket}}{V_{Pellet} + V_{Blanket}}, \tag{2.5}$$

where V_{Pellet} and $V_{Blanket}$ correspond to the total volumes of the fuel pellet and blanket regions, respectively. Similar to equation 2.5, the volume-averaged theoretical density percent provided to FRAPCON (ρ) can be quantified by

$$\rho = \frac{100}{\rho_T(1-\nu)} \left(\rho_{Pellet} \frac{V_{Pellet}}{V_{Pellet} + V_{Blanket}} + \rho_{Blanket} \frac{V_{Blanket}}{V_{Pellet} + V_{Blanket}} \right), \tag{2.6}$$

where ρ_{Pellet} and $\rho_{Blanket}$ are the densities of the pellet and blanket regions, respectively, ρ_T is the theoretical density of UO_2 (10.96 g/cm^3), and ν is the volume-averaged missing-to-total volume ratio of the fuel pellet and blanket regions due to dishes and chamfers.

Fuel pellet dishes and chamfers reduce the volume of the fuel and increase the void volume of the fuel rod and should consequently be considered in the quantification of the RIP and CHS. Chamfers and dishes can also be present in the fuel blanket regions of nuclear fuel. If the fuel densities of the pellet and blanket regions that were utilized in the core simulations of the reactor system result from modeling the fuel pellets as perfect cylinders, the fuel densities need to be inversely-weighted by $1 - \nu$ when modeled with dishes and chamfers in FRAPCON.

Utilizing the values provided by the manufacturer for ν_{Pellet} and $\nu_{Blanket}$, ν can be calculated as

$$\nu = \nu_{Pellet} \frac{V_{Pellet}}{V_{Pellet} + V_{Blanket}} + \nu_{Blanket} \frac{V_{Blanket}}{V_{Pellet} + V_{Blanket}}, \tag{2.7}$$

In FRAPCON-3.5, there can be no axial variations in the fuel pellet design so a representative fuel pellet must be modeled which considers dishes and chamfers that correspond to ν. The missing-to-total volume ratio due to dishes and chamfers can be calculated as

$$\nu = \frac{V_{Dish} + V_{Chamfer}}{\pi r_{Fuel}^2 L_{Pellet}}, \tag{2.8}$$

where V_{Dish} and $V_{Chamfer}$ are the volume reductions (or missing volume) due to fuel dishes and chamfers, respectively. The denominator of equation 2.8 corresponds to the volume of an effective fuel pellet (i.e., a homogenization of the fuel pellet and blanket regions) modeled as a perfect cylinder and r_{Fuel} and L_{Pellet} correspond to the fuel radius and pellet length (or height), respectively.

End dishes are typically modeled as a spherical indentation of radius r_{Dish} to a depth of h_{Dish}. The volume of the dish, V_{Dish}, can be written [8] as

$$V_{Dish} = \pi r_{Dish} h_{Dish}^2 - \frac{h_{Dish}^3}{3}. \tag{2.9}$$

The radius of the dish can be determined from the half chord length l and the depth of the dish:

$$r_{Dish} = \frac{l^2 - h_{Dish}^3}{2h_{Dish}}. \tag{2.10}$$

Fuel dishes are modeled in FRAPCON by specifying two parameters: the depth of the spherical pellet dish (h_{Dish}) and the pellet end-dish shoulder width (w) [9]. It should be noted that in the first revision of the FRAPCON 3.5 manual [9], w is defined as the outer radius of fuel pellet minus the radius of dish. However, this definition is misleading since it implies $w = r_{Fuel} - r_{Dish}$, which is incorrect. A more-appropriate definition of the end-dish shoulder width would be the outer radius of the fuel minus the half chord length of the dish (i.e., $w = r_{Fuel} - l$). By utilizing the proposed definition of w, equation 2.10 may be rewritten as

$$r_{Dish} = \frac{(r_{Fuel} - w)^2 - h_{Dish}^3}{2h_{Dish}}. \tag{2.11}$$

If equation 2.11 is substituted into equation 2.9, w may be written as

$$w = r_{Fuel} - \sqrt{\frac{2V_{Dish}}{\pi h_{Dish}} - \frac{h_{Dish}^2}{3}}. \tag{2.12}$$

In order to utilize equation 2.12 in the FIG, assumptions must be made for h_{Dish} and the portion of the total missing volume that is due to chamfers or dishes. A generic PWR input proposed in [10] utilizes a value 0.0381 cm for h_{Dish} and 10% of the total missing volume is assumed to be due to chamfers (i.e., $\frac{V_{Chamfer}}{V_{Dish}+V_{Chamfer}} = 0.1$).

The chamfered ends of a fuel pellet are modeled as conical frustums, which can be visualized as a slice of a cone taken off parallel to the base. The equation for the volume of the chamfer (i.e., the frustum indentation) is given in [8]:

$$V_{Chamfer} = \pi w_C \left(r_{Fuel}^2 - r_{Fuel} d_C + \frac{1}{3} d_C^2\right), \tag{2.13}$$

where w_C is the width of the chamfer and d_C is the depth of the chamfer. Solving equation 2.13 for w_C yields

$$w_C = \frac{V_{Chamfer}}{\pi r_{Fuel}^2 - \pi r_{Fuel} d_C + \frac{\pi}{3} d_C^2}. \tag{2.14}$$

Similar to pellet dishes, pellet chamfers are modeled in FRAPCON via two input parameters: the chamfer height (d_C) and the chamfer width (w_C). Consequently, assuming a value for d_C and the assumption that $\frac{V_{Chamfer}}{V_{Dish}+V_{Chamfer}} = 0.1$, a corresponding value for w_C may be calculated by the FIG. A chamfer depth of 0.058 cm is assumed in this study, which corresponds to the value used in Calvert Cliffs Unit 1 fuel pellets [11]. A final assumption made regarding the effective fuel pellets that are modeled in FRAPCON is that 272 fuel pellets make up the active fuel length of each fuel rod.

The active fuel length of the fuel rod (L_{Fuel}) is typically kept constant across all fuel assembly batches of a single reactor system. This is observed in the FRAPCON inputs with the exception of fuel rods with annular blankets. In this case, the active fuel length is calculated from the representative perfect cylinder of the fuel and blanket regions. In other words, annular blankets are modeled as shortened cylinders that preserve the fuel volume. Explicitly,

$$L_{Fuel} = \frac{V_{Pellet} + V_{Blanket}}{\pi r_{Fuel}^2}. \tag{2.15}$$

IFBA layers are not modeled in the FRAPCON inputs so IFBA rods are radially equivalent to standard rods at beginning-of-life (BOL). The helium production of the IFBA rods is accounted for by post-processing the FRAPCON outputs to quantify the RIP and CHS.

2.2.3 Fuel Rod Geometry and Fabrication

The radial dimensions of the fuel rod are determined in FRAPCON by three input parameters, the outer diameter of the fuel rod ($D_{O,Rod} = 2r_{O,Clad}$, where $r_{O,Clad}$ is the outer radius of the cladding), the thicknesses of the cladding ($t_{Clad} = r_{O,Clad} - r_{I,Clad}$, where $r_{I,Clad}$ is the inner radius of the cladding), and the fuel-cladding gap ($t_{Gap} = r_{I,Clad} - r_{Fuel}$). A plenum spring can be modeled in FRAPCON by specifying the number of turns, outer spring diameter, and spring wire diameter. The plenum length of each fuel rod is what is specified by the reactor system manufacturer for each assembly batch unless the active fuel length has been shortened due to the presence of annular blankets; for these fuel rods, the cold plenum length is elongated by the difference between the active fuel length provided for the fuel rod and the shortened active fuel length as calculated from equation 2.15. This preserves the void volume of the fuel rods with annular blankets while keeping the total fuel rod length unchanged. The remaining input quantities (fill gas material, fill pressure, and cladding material) require no calculations and are provided from the reactor system manufacturer for each assembly batch.

2.2.4 Irradiation and Operational History

The movements of each fuel rod are modeled across multiple cycles of the chosen reactor system in order to capture its complete irradiation history from BOL to discharge. Once the location of the fuel rod during each fuel cycle has been determined, the volume-averaged LHGR of that location at each time step is read from the text files generated during the pre-processing step into the FRAPCON input. The time steps are typically in units of EFPD and should correspond to what is utilized in the core simulator that generated the fuel rod irradiation histories. This axial mesh utilized in the core simulator can differ from what is required by FRAPCON in order to utilize an axial power profile in a fuel rod input. Specifically, FRAPCON requires that the first element in the axial mesh be zero and the last element be the active fuel length (L_{Fuel}). Because of this, the axial mesh provided by the core simulator may need to be altered so that the first and last elements meet these requirements and all other axial boundaries correspond to the midpoint between the respective nodes of the axial mesh from the core simulator. FRAPCON cannot utilize the axial power profiles of each time step in a single input due to an internal limit to the total number of axial power profile elements [9]. Due to this limitation, a limited number of axial power profiles may be considered for each fuel rod input even though additional profiles are available. If this is the case, axial power profiles are not equally spaced in time in the FIG and are instead chosen based on the time steps since the last power profile was modeled. This method is utilized since it requires no analysis of the total operational history (i.e., the EFPD list) and can be performed quickly in the FIG.

The coolant mass flux (G) of a fuel rod can be calculated from the data provided by the reactor system manufacturer and operator by utilizing the following expression

$$G = \frac{G_{Core}(1-B)}{N_{Assm}} \frac{1}{p_{Assm}^2 - A_{non-coolant}}, \tag{2.16}$$

where G_{Core} is the coolant flow rate of the core, B is the portion of the coolant that bypasses the core, N_{Assm} is the number of assemblies, p_{Assm} is the assembly pitch, and $A_{non-coolant}$ is the cross-sectional area of all fuel rods (A_{Fuel}), guide tubes (A_{GT}), and instrument tubes (A_{IT}). For example, a 17x17 assembly with 24 guide tubes (GT) and a single instrument tube (IT), $A_{non-coolant}$ is given by

$$A_{non-coolant} = 264A_{Fuel} + 24A_{GT} + A_{IT} \tag{2.17}$$

or

$$A_{non-coolant} = 264\pi r_{Fuel}^2 + 24\pi r_{GT}^2 + \pi r_{IT}^2, \tag{2.18}$$

where r_{GT} and r_{IT} are the outer cladding radii of the guide tubes and instrument tubes, respectively. Lastly, the system pressure is provided by the reactor system operator and is typically assumed to be constant across all cycles. No reactor downtimes between fuel cycles are considered in the FIG since warnings are reported in FRAPCON if the power increases or decreases too sharply. It would be undesirable to model a power ramp in these cases because it would alter the irradiation history of the fuel rod predicted by the fuel simulator.

2.2.5 Fission Production of Gaseous Isotopes

Another input quantity used in FRAPCON is the number of He, Kr, and Xe atoms produced per 100 fissions (Γ). The isotopes of interest in the quantification of Γ are the three most common gaseous elements that can be released from nuclear fuel during irradiation. The default value for Γ in FRAPCON-3.5 is 31.0 [9] but care should be taken to quantify Γ for each fuel rod due to its expected effect on RIP predictions. An approximation for the lifetime-averaged value for Γ can be obtained by modeling the fuel rod in SCALE/Polaris, which can perform depletion calculations fuel rod in 2D. Isotopic predictions for the fuel region of the model are calculated by Polaris and are reported in its f71 output file in units of moles per metric ton uranium (MTU). SCALE/Polaris does not contain a fission gas release (FGR) model so the total amounts of He, Kr, or Xe produced in the fuel region throughout irradiation correspond to the isotopic predictions reported by SCALE/Polaris.

At some time of discharge (t), Γ may be quantified by

$$\Gamma(t) = \frac{N_A m_{Fuel}[\mu_{He}(t) + \mu_{Kr}(t) + \mu_{Xe}(t)]}{\int_0^t [\Phi_1(t)\Sigma_{f,1}(t) + \Phi_2(t)\Sigma_{f,2}(t)]dt}, \tag{2.19}$$

where N_A is the Avogadro constant (6.022x10^{23} mol^{-1}), m_{Fuel} is the mass of the fuel rod in MTU, and μ_{He}, μ_{Kr}, and μ_{Xe} correspond to the number of moles per MTU of fuel predicted by Polaris for He, Kr, and Xe, respectively. The denominator in equation 2.19 represents the total number of fissions up to time t where Φ_1 and Φ_2 are the neutron fluxes of the fast and thermal energy groups, respectively, and $\Sigma_{f,1}$ and $\Sigma_{f,2}$ are the macroscopic fission cross sections of the fast and thermal groups for the fuel region, respectively. In FRAPCON-3.5, any neutron with kinetic energy less than 1 MeV is considered to be in the thermal energy range (i.e., group 2). The default thermal energy cutoff in Polaris is 0.625 eV but this value is redefined to correspond to what is utilized in FRAPCON. The integral in the denominator of equation 2.19 can be approximated through the introduction of time steps Δt:

$$\Gamma(t) \cong \frac{N_A m_{Fuel}[\mu_{He}(t) + \mu_{Kr}(t) + \mu_{Xe}(t)]}{\sum_{i=1}^{T} [\Phi_{1,i}\Sigma_{f,1,i} + \Phi_{2,i}\Sigma_{f,2,i}]\, \Delta t_i}, \tag{2.20}$$

where the subscript i serves as the time step index and the total number of time steps is T. All of the values utilized in equation 2.20 are readily available in the Polaris .out or .f71 file so equation 2.20 is used to calculate Γ at any specified burnup corresponding to time t.

2.2.6 Fast Flux Factor

The last quantity to be calculated for use in FRAPCON inputs is the fast flux factor (F_{Fast}), which is the conversion rate between the fast neutron flux and the fuel rod specific power:

$$F_{Fast}(t) = \frac{\Phi_1(t)}{\dot{q}(t)}. \tag{2.21}$$

The default value for F_{Fast} in FRAPCON is 2.21x10^{16} neutrons per square meter per second per W/g of fuel [9]. FRAPCON cannot accept values for F_{Fast} for each time step so a time-weighted sum over the F_{Fast} values ($\bar{F}_{Fast}$) must be calculated and utilized in FRAPCON inputs:

$$\bar{F}_{Fast}(t) = \frac{1}{T}\sum_{i=0}^{N}\frac{\Delta t_i \Phi_{1,i}}{\dot{q}_i}, \tag{2.22}$$

where i is the time step index and T is the time of discharge for the fuel pin, which is separated into N time steps. Similar to Γ, F_{Fast} is calculated individually using equation 2.22 for each fuel rod of the chosen reactor system from representative Polaris cases. If the specific power of the representative Polaris case is constant throughout irradiation, then equation 2.22 may be simplified to yield

$$\bar{F}_{Fast}(t) = \frac{1}{T\dot{q}}\sum_{i=0}^{N}\Delta t_i \Phi_{1,i} = \frac{\bar{\Phi}_i}{\dot{q}}, \tag{2.23}$$

where $\bar{\Phi}_i$ is the time-weighted average of the fast neutron flux.

2.3 Post-Processing

The last step of quantifying the SNF parameters of interest is the post-processing of the FRAPCON output files corresponding to fuel rods with zirconium diboride (ZrB_2) integral fuel burnable absorber (IFBA) layers (referred to as simply "IFBA rods") to account for the helium production from ZrB_2 IFBA layers throughout irradiation. This is necessary because the IFBA model utilized by FRAPCON-3.5 is an empirical expression based on Monte Carlo N-Particle (MCNP) results of an undefined fuel rod model [9]. A higher-fidelity model for the amount of helium released from a ZrB_2 IFBA is utilized in the current work and is derived herein.

Throughout irradiation, a ZrB_2 IFBA layer produces helium gas where the dominant neutron-absorbing reaction is the n-alpha reaction of B-10. Consequently, the rate of helium released from an IFBA layer (dn_{He}/dt) is directly related to the rate of B-10 consumption (dn_{B-10}/dt)

$$\frac{dn_{He}}{dt} = -C_{He,release}\frac{dn_{B-10}}{dt}, \tag{2.24}$$

where $C_{He,release}$ is the probability of an alpha particle being released from the IFBA layer in the fuel void volume. The helium release constant ($C_{He,release}$) is typically assumed to be invariant with time and equal to unity due to the small thickness of ZrB_2 IFBA layers and the mobility of alpha particles. The rate equation of the decay of B-10 in a ZrB_2 IFBA layer can be written as

$$\frac{dn_{B-10}}{dt} = -\sigma_{B-10,n\alpha}\bar{\Phi}n_{B-10}(t), \tag{2.25}$$

where $n_{B-10}(0) = n_{B-10,i}$ and is the amount of boron-10 present in the IFBA layer at BOL, $\bar{\Phi}$ is the average total neutron flux of the system, $n_{B-10}(t)$ is amount of B-10 in the IFBA layer at time t, and $\sigma_{B-10,n\alpha}$ is the microscopic cross-section of the n-alpha reaction of B-10. The form of equation 2.25 implies that the following expression for $n_{B-10}(t)$ is valid

$$n_{B-10}(t) = n_{B-10,i}e^{-\sigma_{B-10,n\alpha}\bar{\Phi}t}. \tag{2.26}$$

The amount of B-10 initially present in an IFBA layer is defined by its axial length (L_{IFBA}) and linear density of B-10 (Λ_{B-10}). Consequently, equation 2.26 can be rewritten as

$$n_{B-10}(t) = L_{IFBA}\Lambda_{B-10}e^{-\sigma_{B-10,n\alpha}\bar{\Phi}t} \tag{2.27}$$

Now, assuming that the only mechanism by which B-10 is destroyed during irradiation is by its n-alpha reaction and $C_{He,release}$ is equal to 1 (i.e., all produced helium is released into the fuel rod void volume), the cumulative amount of helium released at time t can be written as

$$n_{He}(t) = L_{IFBA}\Lambda_{B-10}\left(1 - e^{-\sigma_{B-10,n\alpha}\bar{\Phi}t}\right). \tag{2.28}$$

Equation 2.28 represents the model for the He production of a ZrB_2 IFBA layer in the current work and is a more appropriate model that what is provided in FRAPCON since it takes into account several factors such as the IFBA layer composition ($n_{B-10,i}$), nuclear data ($\sigma_{B-10,n\alpha}$), and the fuel rod irradiation history ($\bar{\Phi}$). Further, the IFBA model utilized in FRAPCON utilizes a fixed helium production rate that is invariant to the initial amount of B-10 that is present in the IFBA layer [9], which is non-physical. In the current project, $\sigma_{B-10,n\alpha}$ is determined by interpolating between pre-determined values for the B-10 n-alpha cross section that are problem-specific to fuel rods with varying enrichments. Equation 2.28 can be rewritten in terms of the fuel burnup (BU) and rod-averaged specific power ($\dot{q}$) to yield

$$n_{He}(t) = L_{IFBA}\Lambda_{B-10}\left(1 - e^{-\sigma_{B-10,n\alpha}\bar{\Phi}\frac{BU}{\dot{q}}}\right). \tag{2.29}$$

If the exponent in equation 2.29 is multiplied and divided by $\bar{\Phi}_1$, equation 2.29 can be rewritten to contain F_{Fast}:

$$n_{He}(t) = L_{IFBA}\Lambda_{B-10}\left(1 - e^{-\sigma_{B-10,n\alpha}F_{Fast}\frac{\bar{\Phi}}{\bar{\Phi}_1}BU}\right). \tag{2.30}$$

A final reorganization of equation 2.30 allows for the quantification of the B-10 utilization factor, β, which corresponds to the amount of B-10 that has been converted into helium relative to the initial loading of B-10.

$$\beta(t) = \frac{n_{He}(t)}{L_{IFBA}\Lambda_{B-10}} = 1 - e^{-\sigma_{B-10,n\alpha}F_{Fast}\frac{\bar{\Phi}}{\bar{\Phi}_1}BU}. \tag{2.31}$$

The B-10 utilization factor provides a simple interpretation of the IFBA helium release model since it is bound between zero and unity, where $\beta = 1$ implies that all B-10 present in the IFBA layer has been converted into gaseous helium.

Since IFBA layers are not modeled in FRAPCON, the RIP and CHS predictions need to be recalculated to account for the increased void gas from an IFBA layer. The total amount of void gas for a fuel rod (n_T) can be calculated as

$$n_T = n_{Fill} + n_{FGR} + n_{He}, \tag{2.32}$$

where n_{He} is the amount of helium released from a ZrB_2 IFBA layer, n_{Fill} is the amount of fill gas, and n_{FGR} is the amount of released fission gas. If it is assumed that the predicted values for n_{Fill} and n_{FGR} would be identical for a fuel rod model with and without an IFBA layer, then n_{Fill} and n_{FGR} can be utilized directly from FRAPCON outputs to calculate n_T for fuel rods with IFBA layers. The RIP (P) for a fuel rod is calculated in FRAPCON by using the ideal gas law

$$P = \frac{(n_{Fill} + n_{FGR} + n_{He})RT}{V}, \tag{2.33}$$

where R is the ideal gas constant (8.314 cm^3MPa/K mol), T is the temperature of the void gas, and V is the total void volume of the fuel rod predicted by FRAPCON. Utilizing equation 2.33 to calculate the RIP of an IFBA rod from a FRAPCON predictions for an identical fuel rod without and IFBA layer has an underlying assumption that the IFBA layer takes up no void volume. This is a minor assumption because IFBA layers have thicknesses ranging from 5 to 15 microns [12], which will minimally affect the total fuel rod void volume.

In addition to the RIP, the CHS must also be recalculated in order to account for the increased RIP. If it is assumed that the RIP has a linear relationship with the CHS, then the following approximation can be applied for quantifying the CHS for rods with IFBA layers (σ_{IFBA}):

$$\sigma_{IFBA} = \sigma_{non-IFBA}\frac{P_{IFBA}}{P_{non-IFBA}}, \tag{2.34}$$

where $\sigma_{non-IFBA}$ and $P_{non-IFBA}$ are the CHS and RIP predictions for an IFBA rod modeled without an IFBA layer in FRAPCON, respectively. Post-processing the FRAPCON outputs in this manner does not take into account the effects an increased RIP or CHS would have on the thermomechanical behavior of the fuel rod during irradiation, however, such as the time-dependent creep rate of the zirconium-based cladding. Consequently, the FRAPCON results of IFBA rods and the RIP and CHS obtained from them by utilizing the proposed IFBA model have limited applicability but are still meaningful with regard to the current work.

3. WATTS BAR NUCLEAR UNIT 1

The reactor system chosen for the current project is Watts Bar Nuclear Unit 1 (WBN1), a Westinghouse-designed pressurized water reactor (PWR). The WBN1 reactor core is composed of 193 fuel assemblies containing fuel rods organized in a 17x17 lattice. Each fuel assembly has 24 guide tubes allowing the insertion of either discrete burnable poisons or a rod cluster control assembly (RCCA). Each assembly also has a central instrument tube (IT) to enable the insertion of a neutron flux detector. WBN1 is currently being modeled on the fuel rod, assembly, and core levels in the VERA Core Physics Benchmark [12]. The guide tube and instrument tube radial orientation is fixed for all assemblies and is displayed in Figure 3.1, which is reproduced from [12]. The fuel rods (shown as gray boxes in Figure 3.1) utilize uranium oxide (UOX) fuel in a 12 ft fuel stack. Each fuel rod contains an upper gas plenum with a plenum spring and upper and lower end plugs. The WBN1 fuel rod arrangement is displayed in Figure 3.2, which is reproduced from [13]. In addition to what is shown in Figure 3.2, there are fuel blanket regions on the top and bottom of the fuel pellet stack. These blanket regions have unique initial fuel enrichments and densities and vary in length between cycles but are several inches long. The fuel blankets may also be annular in order to accommodate an elevated RIP, which is expected for fuel rods with ZrB_2 IFBA layers.

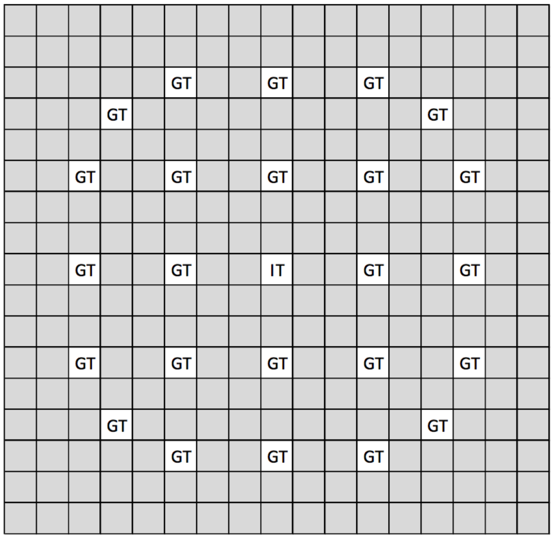

					GT			GT			GT					
			GT										GT			
		GT			GT			GT			GT			GT		
		GT			GT			IT			GT			GT		
		GT			GT			GT			GT			GT		
			GT										GT			
					GT			GT			GT					

Figure 3.1. Radial orientation of WBN1 assemblies [12].

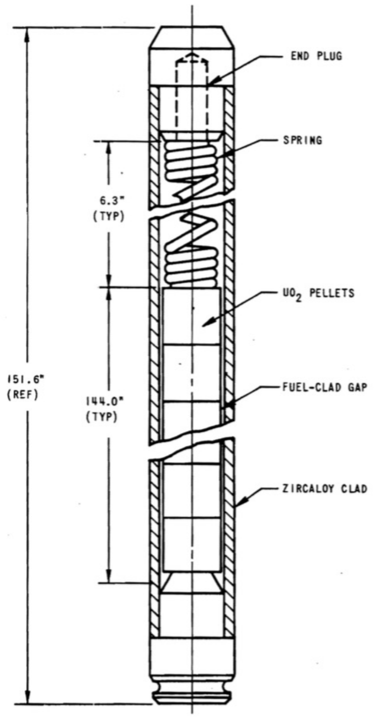

Figure 3.2. Axial arrangement of WBN1 fuel rods [13].

WBN1 is a preferable dataset for quantifying the RIP and CHS distributions of SNF rods due to the extensive amount of data that are available, which describe in detail the operational history, geometry, and initial composition of each fuel rod. The data utilized in this study come from two sources; namely, the assembly manufacturing information, core-level operational history, and inter-cycle assembly movements that are reported by the Tennessee Valley Authority (TVA) and the fuel rod-level operational history data and time-dependent axial power profiles that are calculated as outputs from the core simulations of the VERA multi-cycle benchmarking of WBN1 [14]. These data are available for the first twelve cycles of WBN1, corresponding to over 60,000 unique fuel rod models and operational histories.

3.1 Summary Of Assumptions

One of objectives of the current analysis of WBN1 is to model each WBN1 in as high of detail as possible given the data provided from TVA, and the VERA WBN1 benchmarking [14], but several assumptions must be made in order to perform the analysis. The majority of the assumptions that were made in the current work were described in previous sections but further assumptions must be made when no data are available for the input quantities of interest (e.g., the fuel porosity); in these cases, the default value in FRAPCON is utilized. The following is a list of all of the necessary assumptions that are made during the analysis of WBN1:

1. Fuel rods have homogenized enrichments, densities, and missing-to-total volume ratios (from dishes and chamfers) representative of the fuel pellet and blanket regions.
2. Annular blankets are modeled as shortened cylinders.
3. The number of He, Kr, and Xe atoms produced in the fuel per 100 fissions (Γ) were approximated by trilinear interpolation between what is predicted from the output data of SCALE/Polaris cases, which consider a bounding range of fuel enrichments, lifetime-averaged specific powers, and fuel burnups. A similar assumption is made for the conversion of the fast neutron flux to the fuel

specific power (F_{Fast}) and the ratio of the lifetime-averaged total flux to the lifetime-averaged fast flux ($\bar{\Phi}/\bar{\Phi}_1$)

4. The fuel material is completely non-porous (zero open porosity).
5. The inlet coolant temperature does not vary during a cycle.
6. The WBN1 system pressure and coolant mass flux do not vary over the lifetime of every fuel pin.
7. Axial power profiles are constant during time steps and 20 profiles are sufficient to capture variations throughout fuel rod lifetime.
8. The depth of all dishes is 0.0381 cm.
9. The height of all chamfers is 0.058 cm.
10. The contribution of fuel pellet dishes to the total missing volume is 90%.
11. All gaseous helium produced in a ZrB_2 IFBA layer is released into the fuel rod void volume and the amount is approximated by equation 2.30.
12. The fuel density decreased by 0.1 kg/m^3 during irradiation.
13. No reactor downtime is modeled between subsequent cycles.
14. ZrB_2 IFBA layers do not take up any void volume.
15. The rod-averaged plenum gas temperature for each fuel rod during vacuum drying is 400°C.

These assumptions vary in their implications on RIP and CHS predictions so a brief analysis of their expected effects in warranted. Assumptions 1 and 2 will likely have an effect on RIP and CHS predictions since they factor into the axial temperature distribution of each fuel rod. Care has been taken to ensure that total void volume has been preserved regarding the annular fuel rod blankets but modeling them as shortened cylinders will vary the radial temperature distributions of annular regions. This will likely have a small effect since the annular regions are at the top and bottom of the fuel regions, which have low powers and temperatures relative to the rest of the fuel rod and will consequently not contribute significantly to the amount of released fission gas. The reasoning behind assumption 3 has been discussed in previous sections. Assumption 4 will introduce a positive bias on RIP and CHS predictions because the fuel porosity volume is modeled in FRAPCON and physical uranium oxide fuel has non-zero porosity. However, the fuel open porosity volume is a small portion of the total fuel rod void volume so this will likely have a negligible effect on RIP and CHS predictions. Assumption 5 may have an effect on RIP and CHS predictions since FGR behavior is sensitive to local fuel temperatures, which are dependent on the temperature of the moderator. Assumption 6 is expected to have a negligible effect on RIP and CHS predictions and is a relatively well-known quantity in PWR operation so assuming a fixed value is representative of reality.

Assumption 7 affects the localized fuel temperatures and burnups so it is expected to have an effect of the amount of released fission gas. However, analyses should be performed to determine what level of fidelity is necessary with respect to the number of axial nodes that describe the axial power profile and the number of axial power profiles. The main concern with assumptions 8, 9, and 10 is to preserve the increase in the amount of void volume that is introduced by modeling chamfers and dishes, which is considered and discussed previously. The differences between the physical chamfers and dishes that are present on WBN1 pellets and what is modeling in the current work is expected to have a negligible effect on RIP and CHS predictions. Assumption 11 will have an effect on RIP and CHS predictions of IFBA rods if, in reality, some gaseous helium becomes trapped in the IFBA layer or in the fuel but this seems unlikely due to the motility of alpha particles and the small thickness of IFBA layers. Further, the derivation of the IFBA model assumes that the only means by which B-10 nuclei can interact with incident neutrons is by its n-alpha reaction, which is an assumption that can be made with minimal error since the cross section for this reaction is largely dominating. Assumption 12 will affect the total void volume of a fuel rod (and consequently RIP and CHS predictions) since an increase in this value will result in a more prominent initial decrease in the fuel volume. However, no information for this value was available for WBN1 so the default value in FRAPCON-3.5 is utilized in the current work. The effect of assumption 13 is expected to be minimal since FRAPCON does not model decay heat [9] so an assumed downtime would not affect the fuel composition or the amount of void gas between cycles. Assumption 14 will have a small effect on the total void volume of the fuel rod since IFBA layers are thin so it is expected to have a minimal effect on RIP and CHS predictions. Finally, assumption 15 will directly affect the RIP and consequently the CHS since the RIP with an increased plenum gas temperature. Assuming the maximum temperature for the vacuum drying process implies that the results of the analyses performed in the current work will correspond to conservative (or bounding) predictions. However, additional plenum gas temperatures between 300 and 400°C are also considered when displaying RIP and CHS predictions when analyzing their distributions.

4. RESULTS AND DISCUSSION

All unique fuel rods that were input into the WBN1 core as fresh fuel during cycles 1 through 10 have their specific VERA-predicted operating history, fuel composition, and geometry modeled in FRAPCON. For brevity, these fuel rods will simply be referred to as “cycle 1 through 10 fuel rods”. It is important to note that these fuel rods consider data from twelve cycles of WBN1 since the cycle 10 fuel rods were inserted into the WBN1 core as fresh fuel at cycle 10 but were present during fuel cycles 11 and 12. Fuel rods inserted into the WBN1 core as fresh fuel during cycle 11 and cycle 12 are not considered in the current analysis since their complete irradiation histories are not yet available. Of the cycle 1 through 10 fuel rods, the total number of fuel rods that did and did not contain IFBA layers is approximately 21,000 and 47,000, respectively. All calculated and predicted values shown in this section correspond to vacuum drying conditions of a DSC: an external system pressure (P_{Ext}) of 1 torr (133 Pa) and a void gas temperature (T_f) of 400°C.

In order to maximize the applicability of the results of the current project, the predicted values for the various contributors of the RIP are shown individually in the following sections. To reiterate what was stated in previous sections for clarity, the RIP is quantified in FRAPCON-3.5 by utilizing the ideal gas law:

$$P = \frac{(n_{Fill} + n_{FGR} + n_{He})RT}{V}. \tag{4.1}$$

The purpose of displaying all of the components of equation 4.1 individually is to enable the recalculation of the RIP with different discharge void volume, initial fill pressure, plenum gas temperature, etc. The distributions of Γ, F_{Fast}, and $\bar{\Phi}/\bar{\Phi}_1$ are also analyzed since they either correspond to FRAPCON input quantities or are used in determining the amount of helium produced from IFBA layers. The amount of fill gas (n_{Fill}) is not shown herein because the fill pressure of WBN1 rods is proprietary and could be calculated from n_{Fill} and the non-proprietary WBN1 geometric and fill information. Similarly, the predicted amounts of helium released from IFBA layers (n_{He}) are not shown since, at high-burnups, these values are essentially equivalent to the amount of B-10 loaded onto each IFBA rod, which is proprietary information.

4.1 Operating History

The distribution of discharge fuel burnups for all WBN1 cycle 1 through cycle 10 fuel rods, quantified from VERA-predicted irradiation histories modeled in FRAPCON-3.5, is shown in Figure 4.1 as a histogram over 1,000 burnup bins. Fuel rods that were discharge from the WBN1 core after a single fuel cycle are shown as the peak in Figure 4.1 between 15 and 20 GWd/MTU. From the distribution, it is clear that a considerable portion of the SNF from WBN1 is considered high-burnup (>45 GWd/MTU). The distribution of the peak rod-averaged fuel temperature over the life of each WBN1 fuel rod is shown in Figure 4.2. As is shown in Figure 4.2, the most common peak fuel temperature is about 980 K. The minimum and maximum predicted discharge burnups are 13.5 and 56.0 GWd/MTU, respectively. The minimum and maximum predicted peak rod-averaged fuel temperatures are 710 and 1084 K, respectively. The average of the peak rod-averaged fuel temperatures for standard and IFBA rods is 971 and 976 K, respectively. The distribution of lifetime-averaged LHGRs is shown for all WBN1 cycle 1 through 10 fuel rods in Figure 4.3 where the minimum and maximum LHGR values are 6.67 and 25.29 kW/m, respectively. The average of the lifetime-averaged LHGRs for standard and IFBA rods is 18.15 and 19.79 kW/m, respectively.

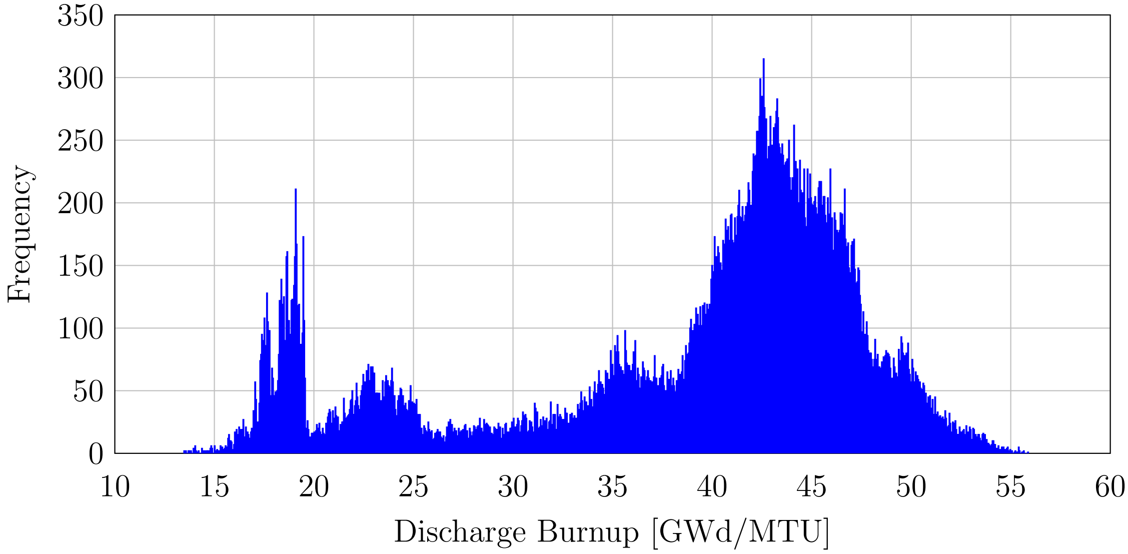

Figure 4.1. The distribution of discharge burnups for cycle 1 through cycle 10 fuel rods.

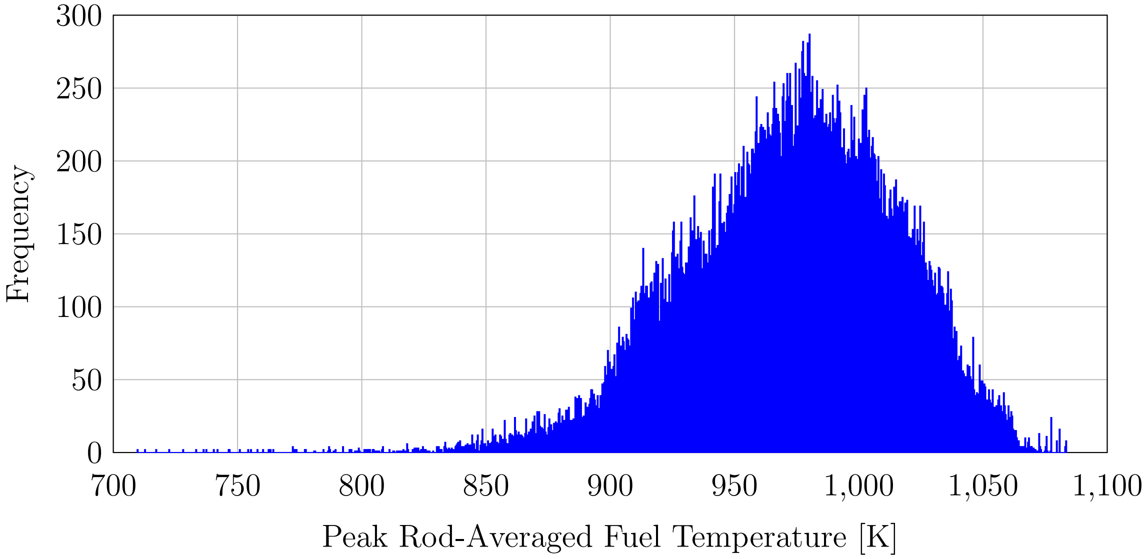

Figure 4.2. The distribution of peak rod-averaged fuel temperatures throughout the lifetimes of WBN1 cycle 1 through cycle 10 fuel rods.

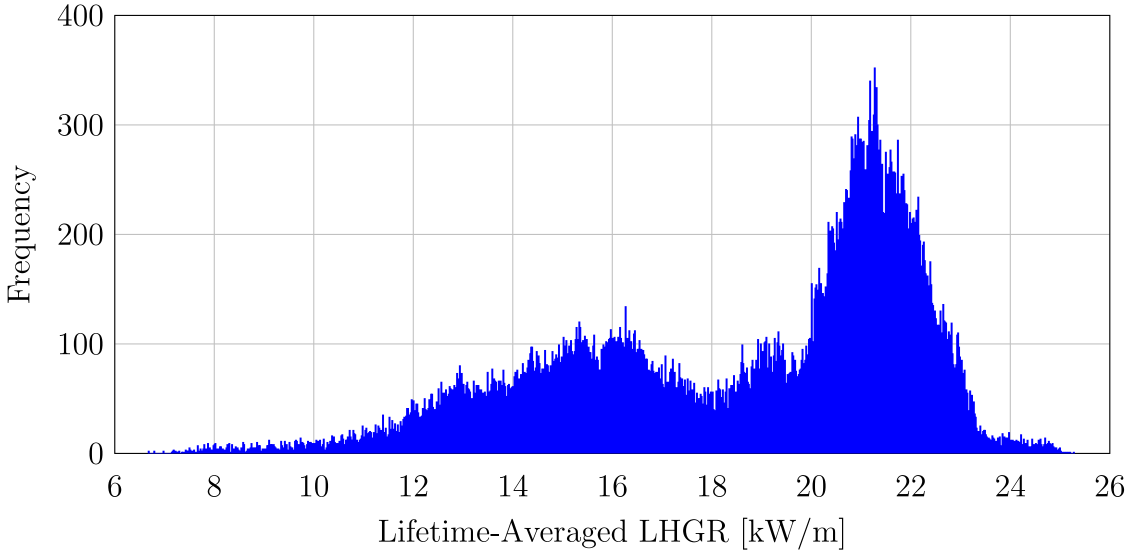

Figure 4.3. The distribution of lifetime-averaged LHGRs of WBN1 cycle 1 through cycle 10 fuel rods.

4.2 FRAPCON Parameters

As discussed previously, values for the number of He, Kr, and Xe atoms produced in the fuel per 100 fissions (Γ) and the conversion between the fast neutron flux and the fuel rod specific power (the fast flux factor, F_{Fast}) need to be calculated from the output parameters of representative Polaris cases. It is impractical to run a Polaris case for each fuel rod of each cycle of WBN1, so Polaris cases were constructed that are representative of a range of fuel enrichments (ε), discharge burnups (BU), and lifetime-averaged specific powers ($\dot{q}$). Once enough predictions of Γ were quantified, the behavior of Γ due to variations in these quantities could be approximated. In order to investigate the behavior of Γ, it is necessary to compare predicted values of Γ as a function of each input quantity. Using a pre-release version of SCALE6.2, a WBN1 pin cell was modeled in Polaris with a fixed specific power of 40 W/g and an initial enrichment of 3.0 wt.% U-235. The nuclear data library used in this analysis and all subsequent Polaris analyses was a 252-group library generated from ENDF/B-VII.1 data.

The predicted values for Γ correspond to burnups ranging from 10 to 62 GWd/MTU and are calculated using equation 2.20 and are displayed in Figure 4.4. As is shown, Γ increases with fuel burnup at a rate that decreases with increasing burnup. This is reasonable since He, Kr, and Xe are not present in WBN1 fresh fuel and accumulate during irradiation. The slowdown in the rate of increase of Γ can justified by considering that some of the isotopes considered, mainly the xenon isotopes, decay at a rate that is comparable to the rate they are being produced. Due to this, the amount of Xe present in WBN1 fuel increases rapidly at times near BOC and eventually reaches an equilibrium concentration once the fuel has been continuously irradiated for a long enough duration. Based on the data shown in Figure 4.4, if the burnup mesh is kept fine enough, Γ can be approximated by linear interpolation between two subsequent burnups. The linear interpolation between each burnup step is displayed as the red line in Figure 4.4. If enrichment and specific power were fixed across all fuel rods, linear interpolation between Γ predictions at various burnups would be a reasonable way to estimate Γ. However, the initial fuel enrichment and lifetime-averaged specific powers will vary considerably across all WBN1 pins so the behavior of Γ with respect to enrichment and specific power should also be assessed.

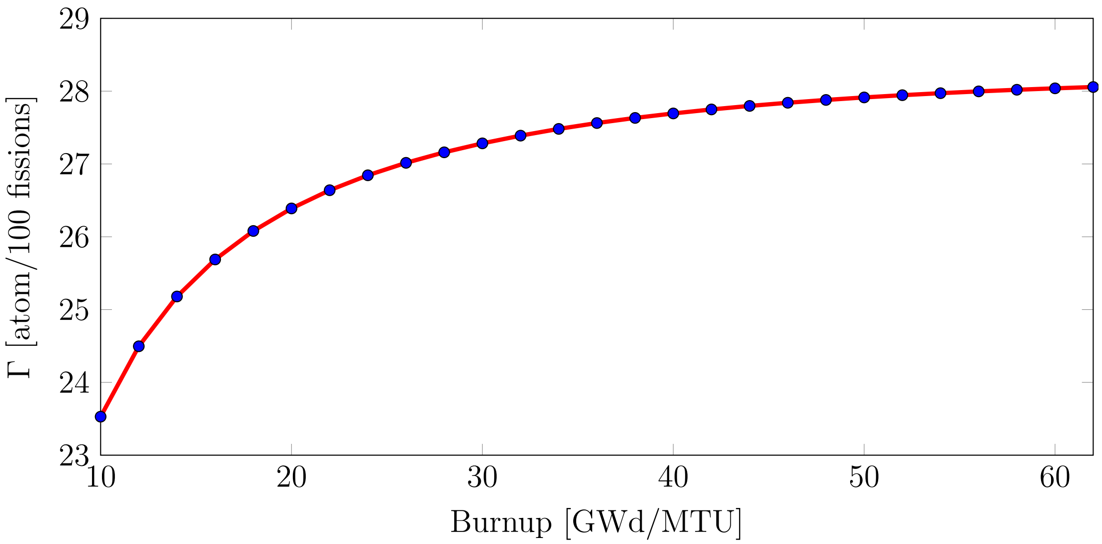

Figure 4.4. Predictions of Γ calculated from SCALE/Polaris output data using equation 2.20. The fuel specific power was kept constant at 40 W/g and the initial enrichment was 3 wt.% U-235.

In order to assess the behavior of Γ with variations in the initial enrichment, four WBN1 fuel pin Polaris models are utilized with enrichments of 2, 3, 4, and 5 wt.% U-235 and a fixed specific power of 40 W/g. Predictions for Γ for these four cases are shown in Figure 4.5 and reveal that as enrichment increases, Γ decreases. The data shown in Figure 4.5 correspond to a fuel burnup of 60 GWd/MTU. The decrease in Γ with an increasing enrichment is reasonable because as the enrichment increases, the number of fissions will increase while the mean neutron energy increases. The cumulative effect of these two behaviors is a decrease in the amount of He, Kr, and Xe atoms that are being produced because they are less likely to be produced from fission reactions caused by a higher-energy neutron. Figure 4.5 also shows that approximating Γ by linear interpolation with respect to variations in the initial enrichment is a valid approximation. It should be noted that the decrease of Γ with increasing initial enrichment is observed across all considered fuel burnups.

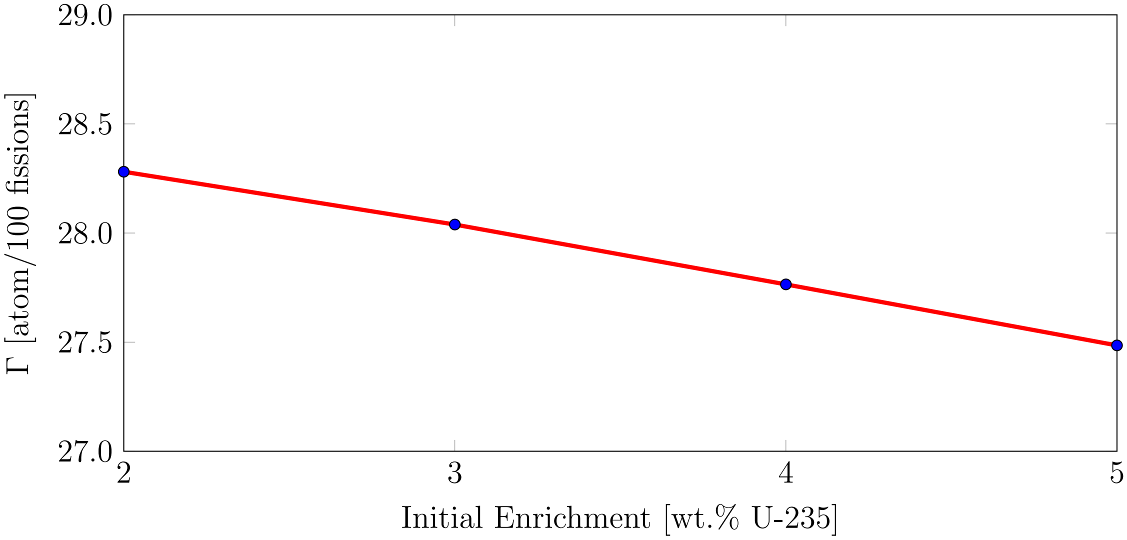

Figure 4.5. Predictions of Γ calculated from SCALE/Polaris output data using equation 2.20 with a constant specific power of 40 W/g evaluated at a fuel burnup of 60 GWd/MTU.

The behavior of Γ with respect to the lifetime-average specific power can be assessed from the output data of SCALE/Polaris WBN1 models that only vary in their fuel specific power. Predicted values of Γ from five models are compared, which utilize specific powers of 10, 20, 30, 40, and 50 W/g with a fixed initial enrichment of 3 wt.% U-235 and discharge burnup of 60 GWd/MTU, and are shown in Figure 4.6. The behavior of Γ with respect to specific power is not as linear as it was for the initial enrichment but it can be approximated as linear within specific power changes of the considered magnitude (10 W/g). The increase in Γ with increasing specific power is justifiable since more fission products are being produced in the fuel, which includes He, Kr, Xe, and each of their precursors.

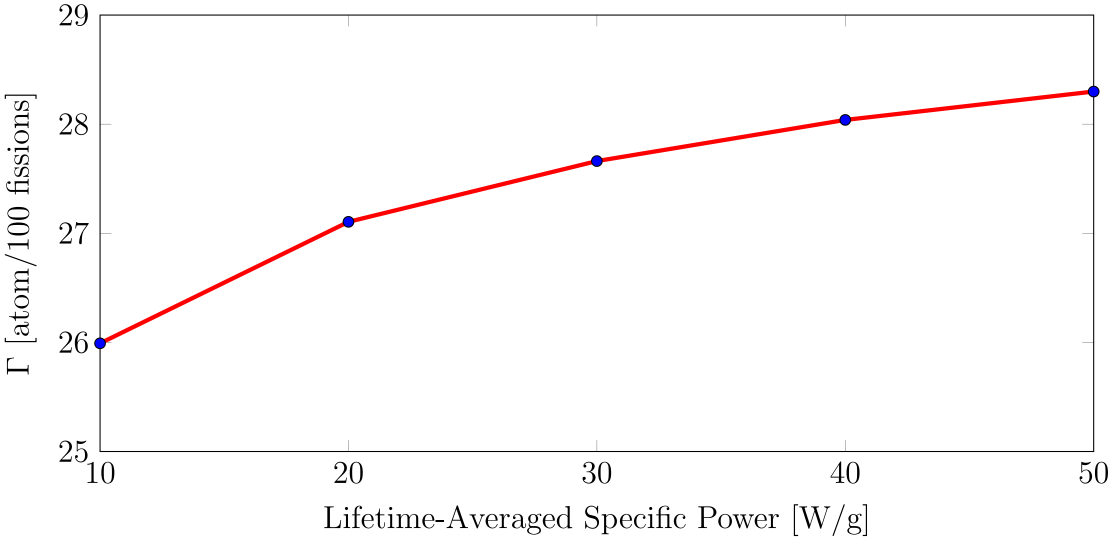

Figure 4.6. Predictions of Γ calculated from SCALE/Polaris output data using equation 2.20 with an initial enrichment of 3 wt.% U-235 evaluated at a fuel burnup of 60 GWd/MTU.

Based on the analyses of the behavior of Γ explained above, a reasonable way to approximate Γ is by trilinear interpolation between a series of pre-calculated values that encompass of a range of initial enrichments, fuel burnups, and fuel specific powers. Twenty Polaris cases are considered with initial enrichments of 2, 3, 4, and 5 wt.% U-235 and specific powers of 10, 20, 30, 40, and 50 W/g. Each Polaris input contains output data for fuel burnups ranging from 0 to 62 GWd/MTU with a burnup increment equal to one GWd/MTU. Predictions for Γ are calculated using 2.20 at each initial enrichment, specific power, and burnup combination, which is meant to represent the total space of possible values for WBN1 fuel rods with respect to these quantities. Explicitly, once the enrichment, lifetime-averaged specific power, and burnup are known for a WBN1 fuel pin, the eight predictions for Γ, which surround the fuel rod in terms of enrichment, specific power, and burnup are determined. This can be visualized in Figure 4.7, which is reproduced from [15] where p is the prediction to be quantified and p_{000} through p_{111} represent the pre-calculated values of the parameter that surround the prediction.

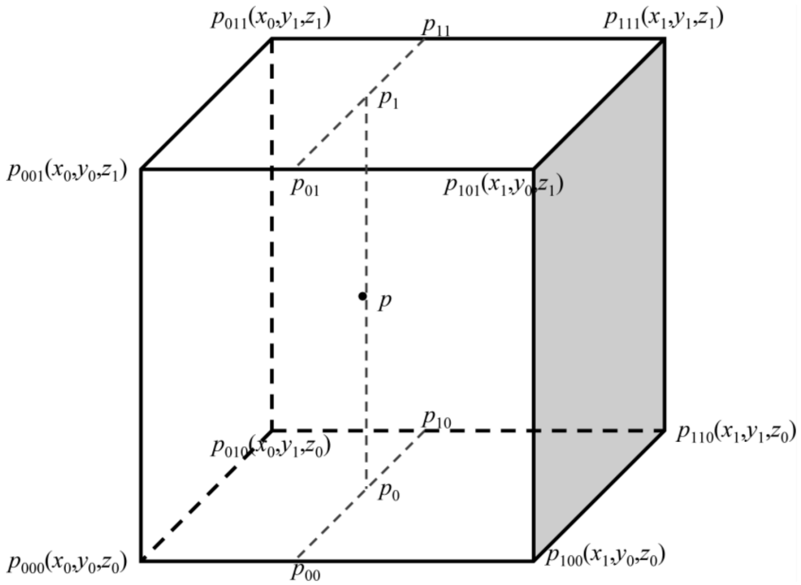

Figure 4.7. A visualization of trilinear interpolation where the desired prediction p lies between eight pre-calculated data points [15].

Trilinear interpolation across the three dimensions of initial enrichment (ε), specific power ($\dot{q}$), and burnup (BU) in order to determine $\Gamma(\varepsilon, \dot{q}, BU)$ can be written as

$$\begin{aligned}\Gamma(\varepsilon, \dot{q}, BU) \; = \mathrm{c}_0 + \mathrm{c}_1\Delta\varepsilon + \mathrm{c}_2\Delta\dot{q} + \mathrm{c}_3\Delta\mathrm{BU} + \mathrm{c}_4\Delta\varepsilon\Delta\dot{q} + \\ \mathrm{c}_5\Delta\dot{q}\Delta\mathrm{BU} + \mathrm{c}_6\Delta\varepsilon\Delta\mathrm{BU} + \mathrm{c}_7\Delta\varepsilon\Delta\dot{q}\Delta\mathrm{BU},\end{aligned} \tag{4.2}$$

where

$$\begin{aligned}\Delta\varepsilon &= (\varepsilon - \varepsilon_0)/(\varepsilon_1 - \varepsilon_0)\\ \Delta\dot{q} &= (\dot{q} - \dot{q}_0)/(\dot{q}_1 - \dot{q}_0)\\ \Delta\mathrm{BU} &= (\mathrm{BU} - \mathrm{BU}_0)/(\mathrm{BU}_1 - \mathrm{BU}_0)\end{aligned} \tag{4.3}$$

and

$$\begin{aligned}c_0 &= \Gamma_{000}\\ c_1 &= \Gamma_{100} - \Gamma_{000}\\ c_2 &= \Gamma_{010} - \Gamma_{000}\\ c_3 &= \Gamma_{001} - \Gamma_{000}\\ c_4 &= \Gamma_{110} - \Gamma_{010} - \Gamma_{100} + \Gamma_{000}\\ c_5 &= \Gamma_{011} - \Gamma_{001} - \Gamma_{010} + \Gamma_{000}\\ c_6 &= \Gamma_{101} - \Gamma_{001} - \Gamma_{100} + \Gamma_{000}\\ c_7 &= \Gamma_{111} - \Gamma_{011} - \Gamma_{101} - \Gamma_{110} + \Gamma_{100} + \Gamma_{001} + \Gamma_{010} - \Gamma_{000}.\end{aligned} \tag{4.4}$$

Equations 4.2, 4.3, and 4.4 form the foundation for approximating a quantity by trilinear interpolation for the current work. In order to ensure that the Polaris cases are representative of the WBN1 fuel rods, the representative Polaris cases are modeled twice: once with and without an IFBA layer. If the WBN1 fuel rod has an IFBA layer, then Γ is interpolated between the pre-calculated values, which also considered an IFBA layer in Polaris. The distribution of predicted values for Γ cycle 1 through cycle 10 fuel rods of WBN1 is shown in Figure 4.8 as a histogram of 1,000 bins. The predictions for Γ shown in Figure 4.8 indicate that a Γ value between 26 and 27 is likely for a WBN1 fuel rod. Given the behavior of Γ with fuel burnup shown in Figure 4.4 and the distribution of fuel burnups shown in Figure 4.1, the lower values of Γ correspond to fuel rods with lower burnups. Consequently, a fuel rod with a high discharge fuel burnup (>45 GWd/MTU) will likely have a Γ near 27 while lower burnup rods will have Γ values ranging from 23.5 to 27, according to Polaris output data.

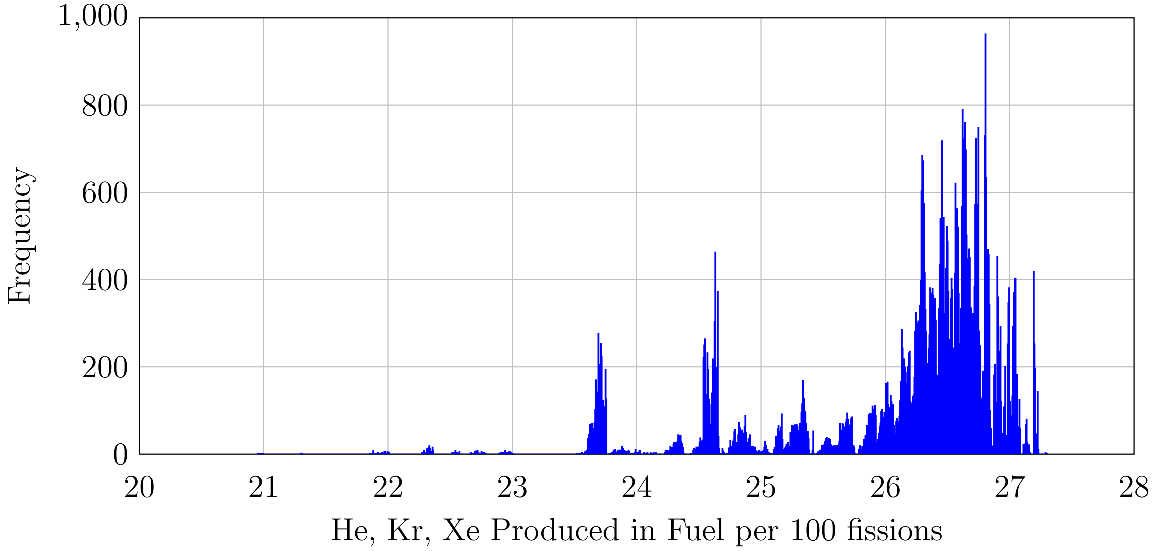

Figure 4.8. The distribution of Γ predictions for WBN1 cycle 1 through cycle 10 fuel rods calculated from SCALE/Polaris output data using equation 2.20.

The same Polaris output data that are used to determine the behavior of Γ are used with equation 2.23 to determine F_{Fast}. The behavior of F_{Fast} with respect to changes in burnup, initial enrichment, and lifetime-averaged specific power are shown in Figures 4.8, 4.9, and 4.10, respectively. The gradual increase of F_{Fast} with respect to burnup, shown in Figure 4.9, is understandable because as the fuel is depleted the amount of U-235 decreases, which causes the flux necessary to maintain the fixed specific power to increase. This effect is augmented since the mean neutron energy increases during depletion. The decrease of F_{Fast} with increasing fuel enrichment, shown in Figure 4.10, is expected because as the enrichment of the fuel increases, the total flux required for the fuel to reach a fixed specific power will decrease. This results in a net increase in the predicted value for F_{Fast} despite the fact that the normalized fast flux will increase with an increasing enrichment due to the increased thermal absorption by U-235. The increase in F_{Fast} with an increasing specific power, shown in Figure 4.11, is expected since the total flux will increase in order to produce the increased specific power when all other input quantities are fixed. Lastly, the strong linear behavior of F_{Fast} shown in Figures 4.8, 4.9, and 4.10 support the method of approximating F_{Fast} by trilinear interpolation with respect to initial enrichment, lifetime-averaged specific power, and burnup. The distribution of F_{Fast} predictions for WBN1 cycle 1 through cycle 10 fuel rods is shown in Figure 4.12 as a histogram of 1,000 bins.

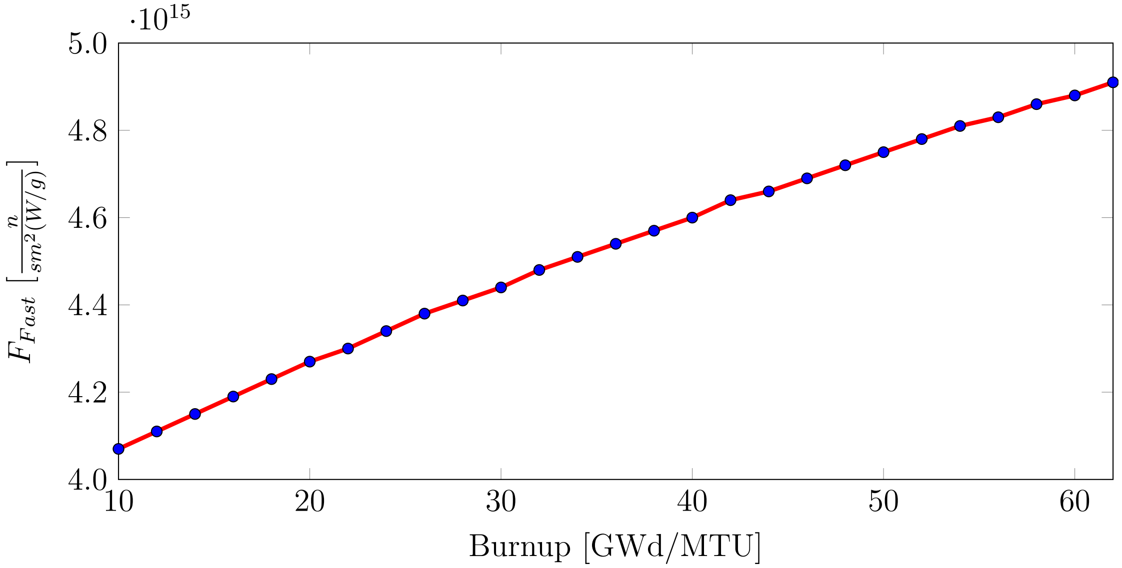

Figure 4.9. Predictions of F_{Fast} calculated from SCALE/Polaris output data using equation 2.23. The fuel specific power was kept constant at 40 W/g and the initial enrichment was 3 wt.% U-235.

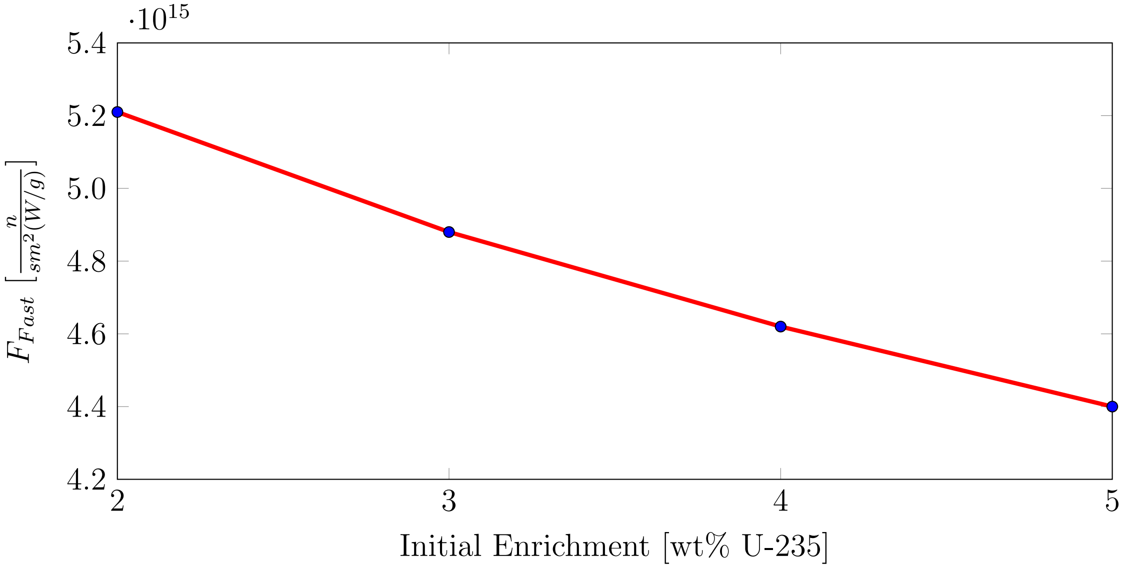

Figure 4.10. Predictions of F_{Fast} calculated from SCALE/Polaris output data using equation 2.23. The fuel specific power and burnup correspond to 40 W/g and 60 GWd/MTU, respectively.

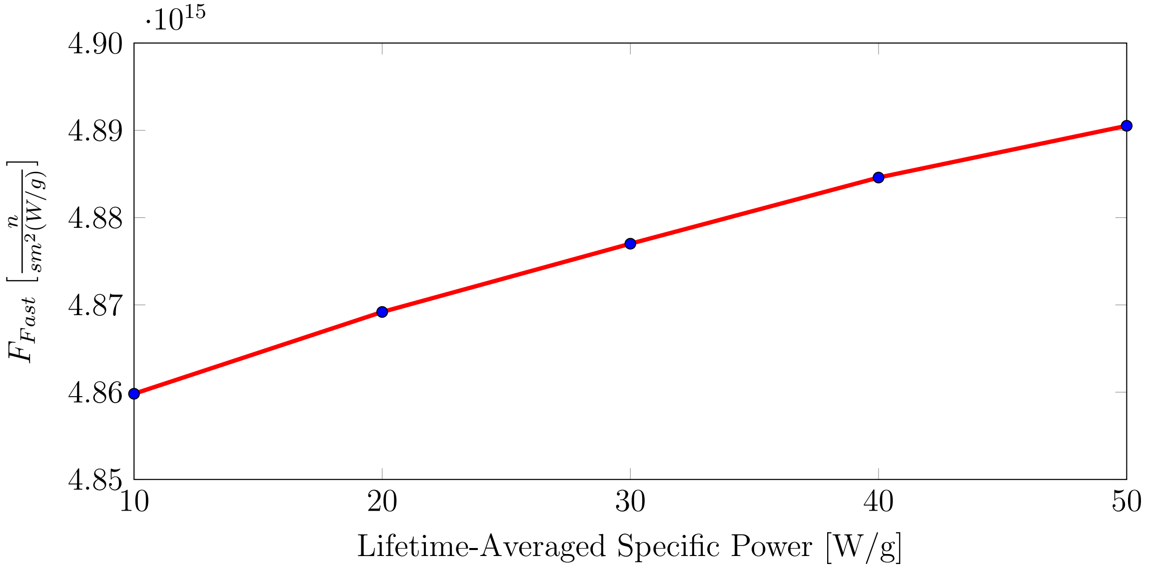

Figure 4.11. Predictions of F_{Fast} calculated from SCALE/Polaris output data using equation 2.23. The fuel specific power and initial enrichment correspond to 40 W/g and 3 wt.% U-235, respectively.

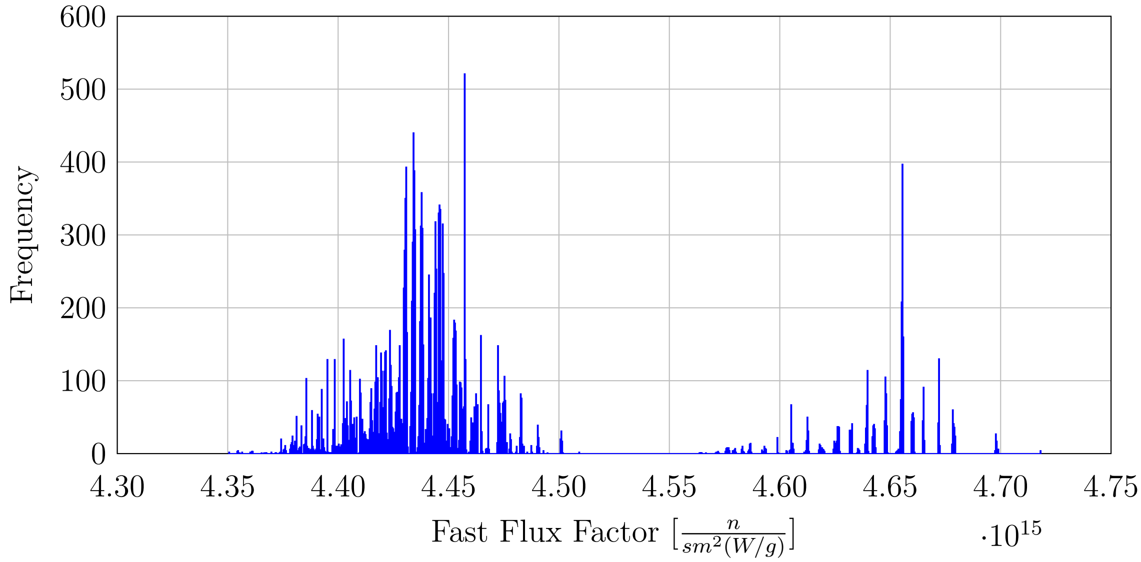

Figure 4.12. The distribution of predicted values for F_{Fast} calculated from SCALE/Polaris output data using equation 2.23.

The results shown in Figure 4.12 elucidate the difference between F_{Fast} predictions of standard and IFBA rods: where IFBA rods have generally higher F_{Fast} predictions. This can be understood by recalling that IFBA rods often have annular blanket regions, which decrease the mass of the fuel present in the fuel rod and that IFBA rods are generally placed in high power regions of the assembly. This will result in an elevated lifetime-averaged specific power for the IFBA rods when compared to standard rods. Given the behavior of the F_{Fast} with respect to the specific power shown in Figure 4.11, an increased specific power will result in a higher prediction of F_{Fast}, which is observed in Figure 4.12 for IFBA rods. Given the distribution shown in Figure 4.12, standard rods will have a F_{Fast} near 4.44x10^{15} n/sm^2 per W/g fuel while IFBA rods will have a F_{Fast} value near 4.65x10^{15} n/sm^2 per W/g fuel according to Polaris output data.

It is acceptable to assume that $\bar{\Phi}/\bar{\Phi}_1$ is approximately linear with respect to burnup, enrichment, and specific power due to the results of the homologous analysis of F_{Fast}, which showed that this was a reasonable approximation for $\bar{\Phi}_1$. Consequently, the factor of $\bar{\Phi}/\bar{\Phi}_1$ can be determined by trilinear interpolation between pre-calculated values from the same SCALE/Polaris models that are used to approximate Γ and F_{Fast}. The distribution of predicted values for $\bar{\Phi}/\bar{\Phi}_1$ is shown in Figure 4.13 as a histogram of 1,000 bins. Similar to the distribution of F_{Fast} predictions (see Figure 4.12), the distribution of $\bar{\Phi}/\bar{\Phi}_1$ values is unique for fuel rods with and without an IFBA layer. Explicitly, $\bar{\Phi}/\bar{\Phi}_1$ will be centered around 1.665 and 1.695 for standard and IFBA rods, respectively. It is evident from IFBA $\bar{\Phi}/\bar{\Phi}_1$ predictions that the fast flux makes up a smaller portion of the total flux compared to that of standard rods. This is understandable since the thermal absorption of the IFBA layer decreases the number of U-235 fissions, which decreases the amount of fast neutrons in the fuel rod model.

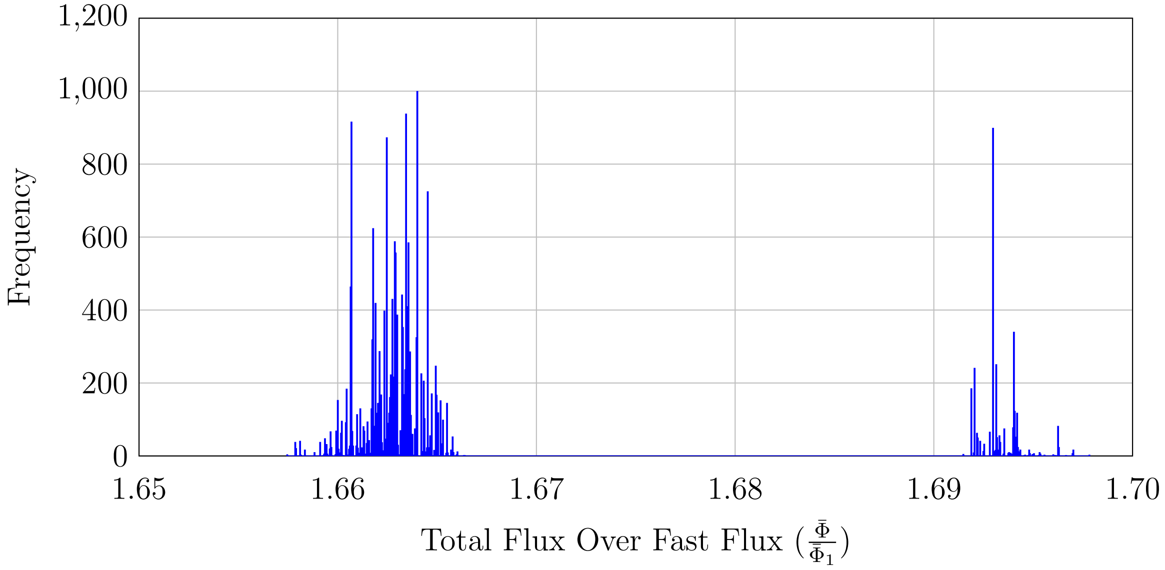

Figure 4.13. The distribution of predicted values for total flux over the fast flux calculated from SCALE/Polaris output data.

4.3 Total Fuel Rod Void Volume

The total void volume and fuel burnup at time of discharge for each standard and IFBA fuel rod that were fed as fresh fuel into WBN1 during cycles 1 through 10 are shown in Figure 4.14 with the density of data shown in Figure 4.15. To give more detail on the generation of Figure 4.15, the range of discharge burnups are divided into 100 bins, then the range of void volume predictions in each bin are determined and divided into 100 bins; the resulting 10,000 data points are then plotted as void volume versus burnup with a logarithmic color scale corresponding to the frequency of data in each bin. The IFBA rods without annular fuel blankets can be clearly seen in Figure 4.14 as the only IFBA data with void volumes that overlap those of the standard rods. The majority of standard rods that were discharged from the WBN1 core after just a single cycle have their void volumes centered on a small region between 15 and 20 GWd/MTU, which is displayed as the high-density region in Figure 4.15. IFBA rods discharged after a single cycle are also visible in Figure 4.14 and Figure 4.15 between burnups of 15 and 25 GWd/MTU. The void volume differences of the IFBA data are due to the utilization of annular blankets of different lengths. The distribution of total void volumes for all cycle 1 through 10 fuel rods is shown in Figure 4.16 as a histogram over 1,000 bins. The data shown in Figure 4.16 imply that the most common discharge void volume for standard and IFBA rods is about 14.5 cm^3 and 19.2 cm^3, respectively. The minimum and maximum predictions for the final void volume are 12.33 and 20.67 cm^3, respectively.

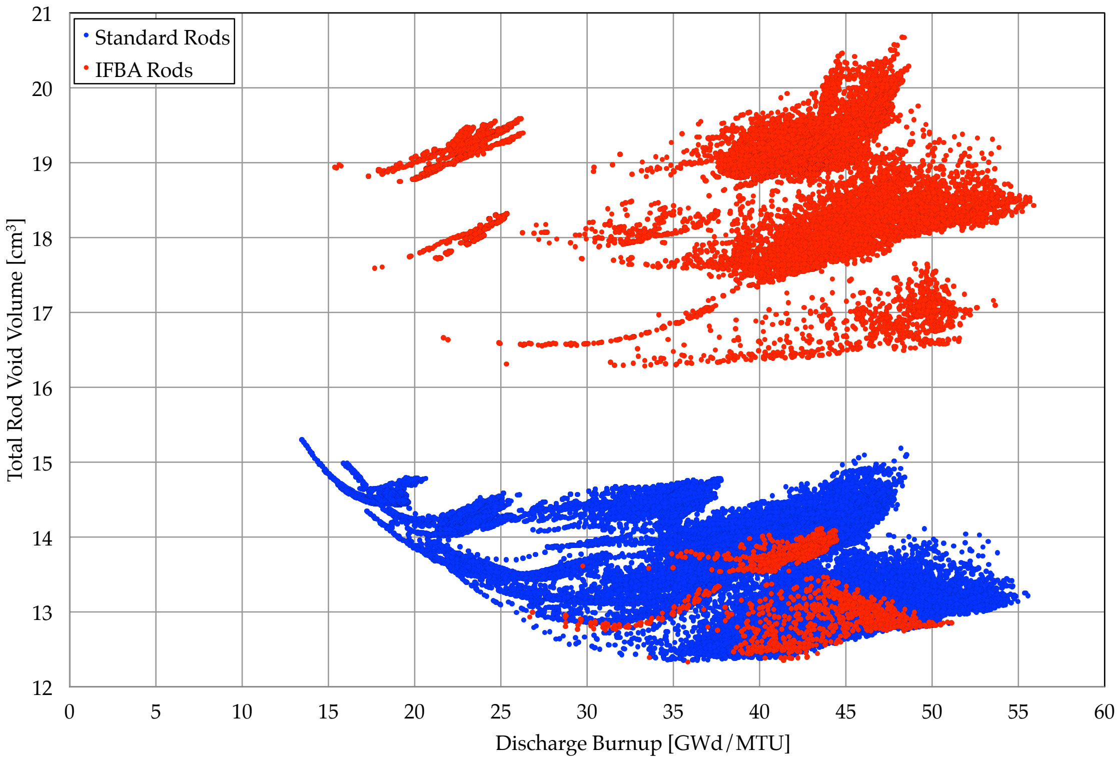

Figure 4.14. Total void volume predictions for cycle 1 through cycle 10 fuel rods under vacuum drying conditions (P_{Ext}=133 Pa, T_F=400°C).

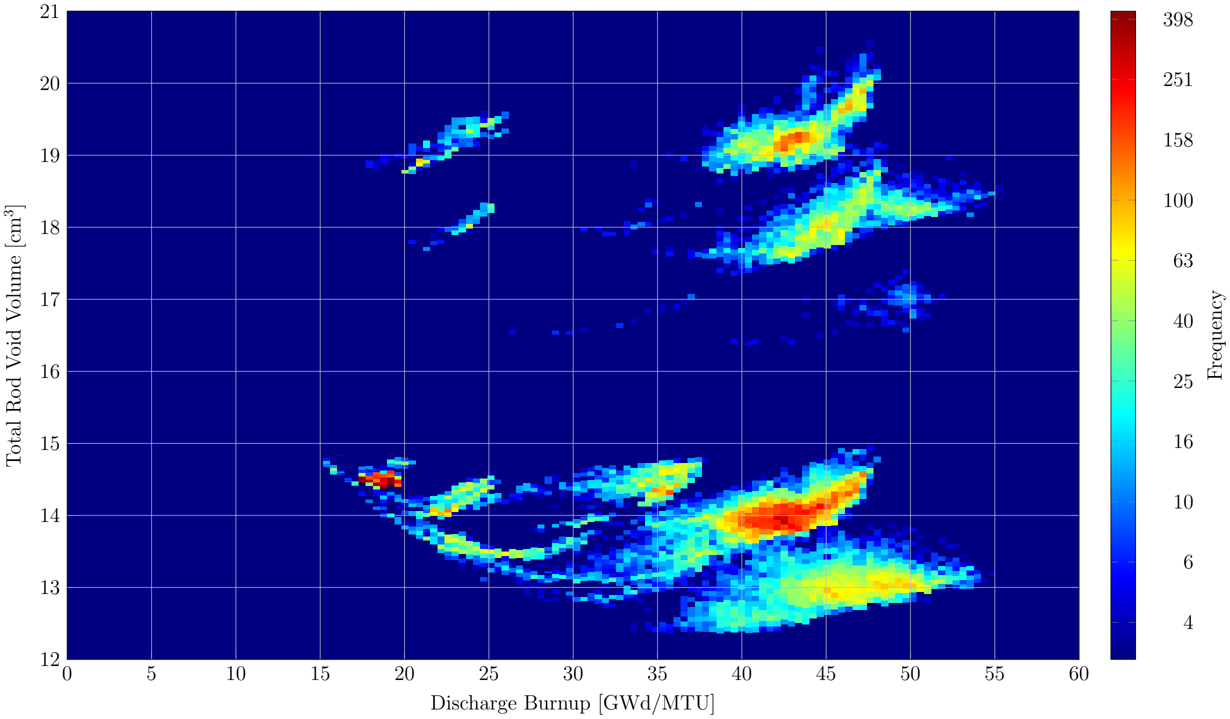

Figure 4.15. Total void volume predictions for cycle 1 through cycle 10 fuel rods under vacuum drying conditions (P_{Ext}=133 Pa, T_F=400°C). Colors correspond to the amount of data within each discharge burnup and void volume bin.

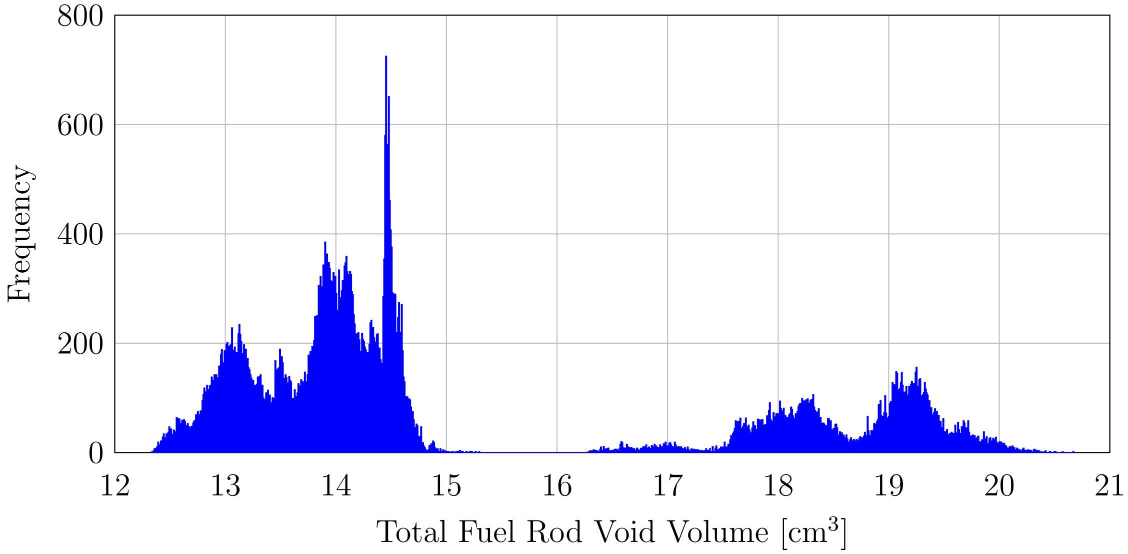

Figure 4.16. The distribution of total void volume predictions for cycle 1 through cycle 10 fuel rods under vacuum drying conditions (P_{Ext}=133 Pa, T_F=400°C).

The predicted void volume of each WBN1 fuel rod (V_f) can also be shown relative to the initial void volume (V_i), which corresponds to the fuel rod at fill conditions. The corresponding V_f/V_i ratios are shown in Figure 4.17 with the distribution shown in Figure 4.18 as a histogram of 1,000 bins. The minimum and maximum predictions for V_f/V_i are 0.600 and 0.814, respectively.

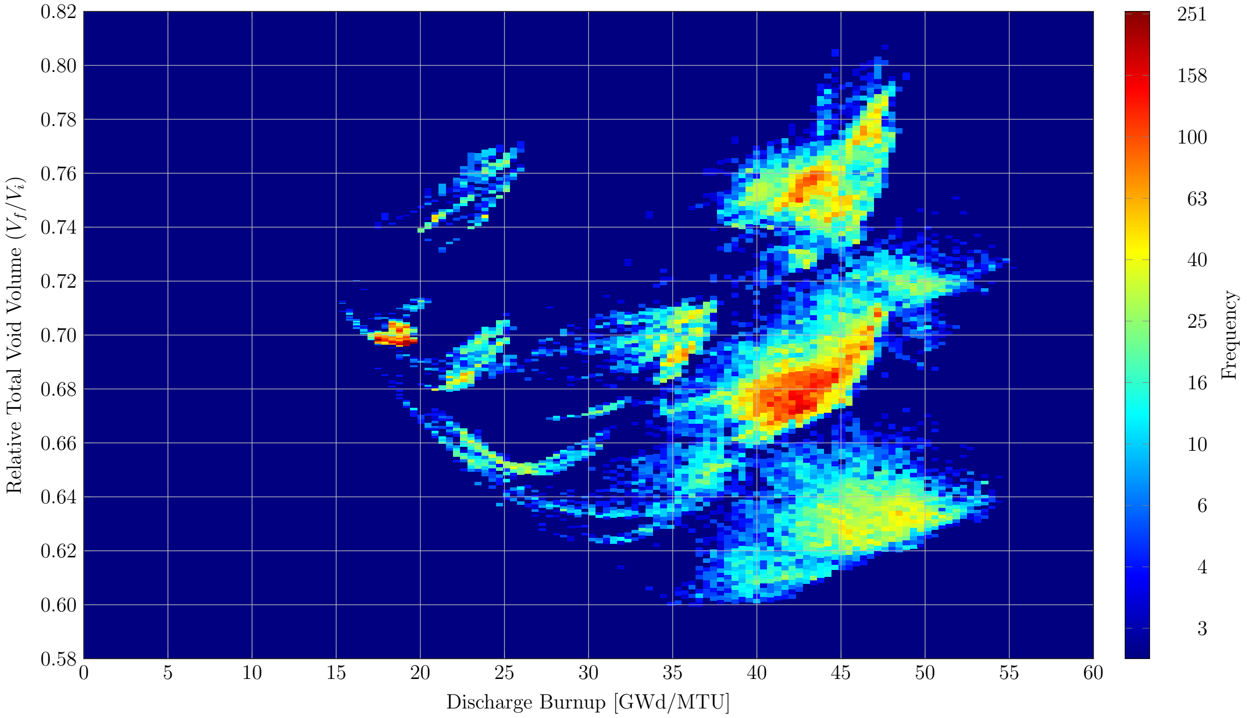

Figure 4.17. Relative void volume predictions (V_f/V_i) for cycle 1 through cycle 10 fuel rods under vacuum drying conditions (P_{Ext}=133 Pa, T_F=400°C). Colors correspond to the amount of data within each discharge burnup and void volume bin.

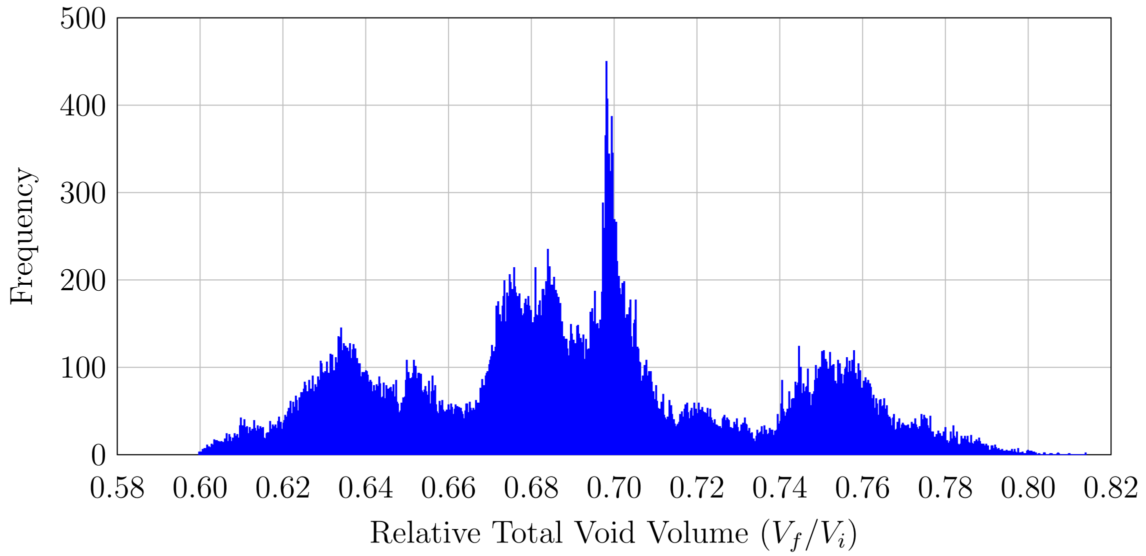

Figure 4.18. The distribution of relative void volume predictions (V_f/V_i) for cycle 1 through cycle 10 fuel rods under vacuum drying conditions (P_{Ext}=133 Pa, T_F=400°C).

4.4 Released Fission Gas

The amount of released fission gas in moles is shown with respect to the discharge burnup in Figure 4.19 and the density of the data is shown in Figure 4.20. It is clear from the data shown in Figure 4.19 that the highest predictions for n_{FGR} correspond to fuel rods with IFBA layers. A brief analysis of the IFBA rods with the highest amounts of released fission gas reveals that these rods experience higher fuel temperatures than standard rods. This is understandable because IFBA rods have a higher peak rod-averaged fuel temperatures and lifetime-averaged LHGRs on average than standard rods (975.8 versus 970.9 K and 19.79 versus 18.15 kW/m, respectively). IFBA rods on average have higher fuel temperatures than non-IFBA rods since they are placed in high-power regions of the assembly. Due to the increased fuel temperatures of IFBA rods, the amount of released fission gas is expected to increase because these rods are more likely to exceed the Vitanza threshold temperature for the transition from athermal to burst fission gas release behavior [2]. This transition is not explicitly modeling in FRAPCON-3.5, where instead a released fission gas prediction is calculated from a high-temperature model (modified Forsberg-Massih) and a low-temperature model and the higher of the two predictions is utilized [9]. Additionally, cursory investigations reveal that as F_{Fast} increases, the local burnup required to transition to burst FGR behavior in FRAPCON decreases. Since IFBA rods have higher predicted values for F_{Fast} than standard rods, they experience burst FGR behavior at lower burnups than standard rods, which supports what is observed in Figure 4.19. It can be concluded from the data shown Figure 4.20 that the majority of cycle 1 through 10 fuel rods of WBN1 remain in the low-temperature model for FGR. The distribution of released fission gas also supports this conclusion and is shown in Figure 4.21 as a histogram over 1,000 bins. The minimum and maximum predictions for the amount of released fission gas is 8.92x10^{-5} and 6.67x10^{-3} mol, respectively.

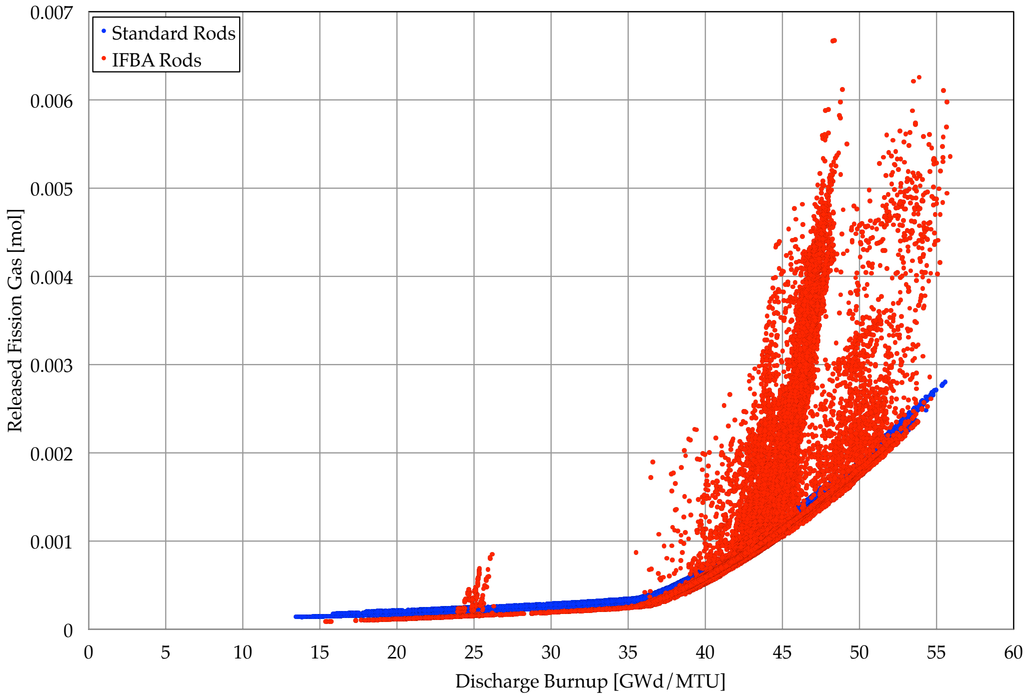

Figure 4.19. Released fission gas predictions for cycle 1 through cycle 10 fuel rods of WBN1.

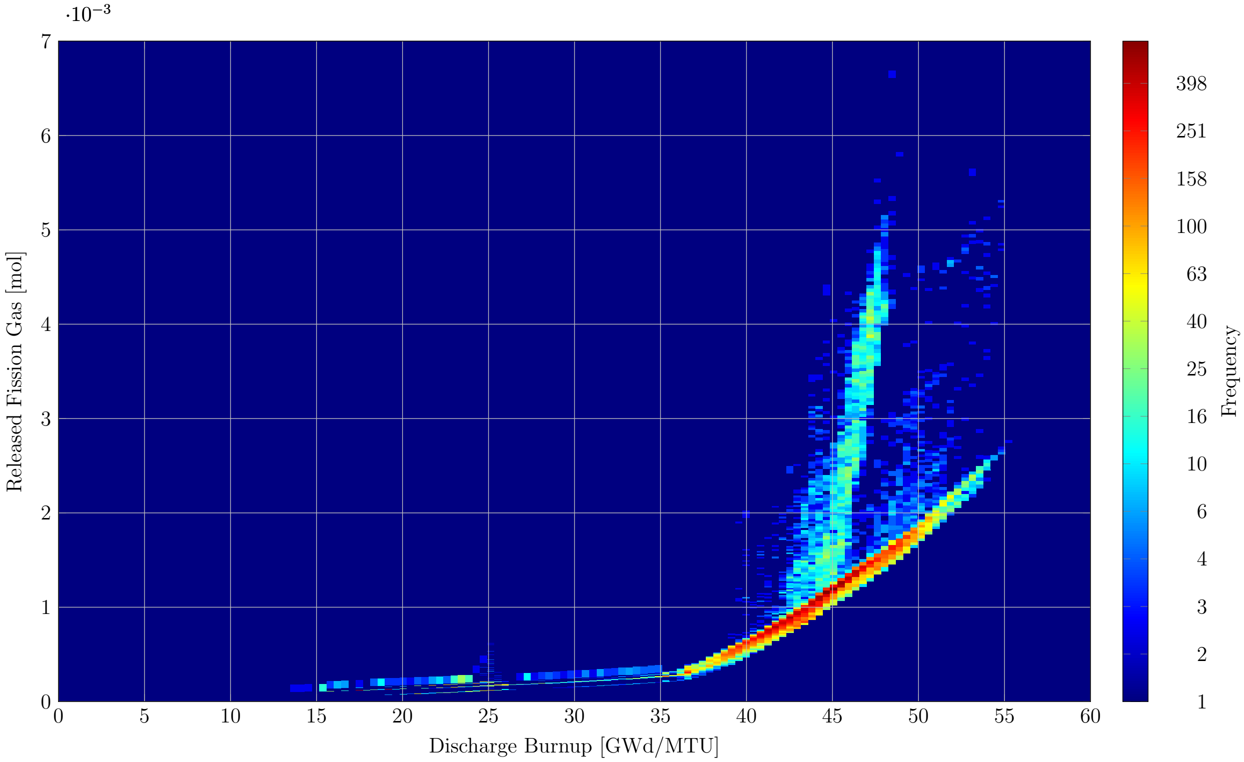

Figure 4.20. Released fission gas predictions for cycle 1 through cycle 10 fuel rods of WBN1. Colors correspond to the amount of data within each discharge burnup and released fission gas bin.

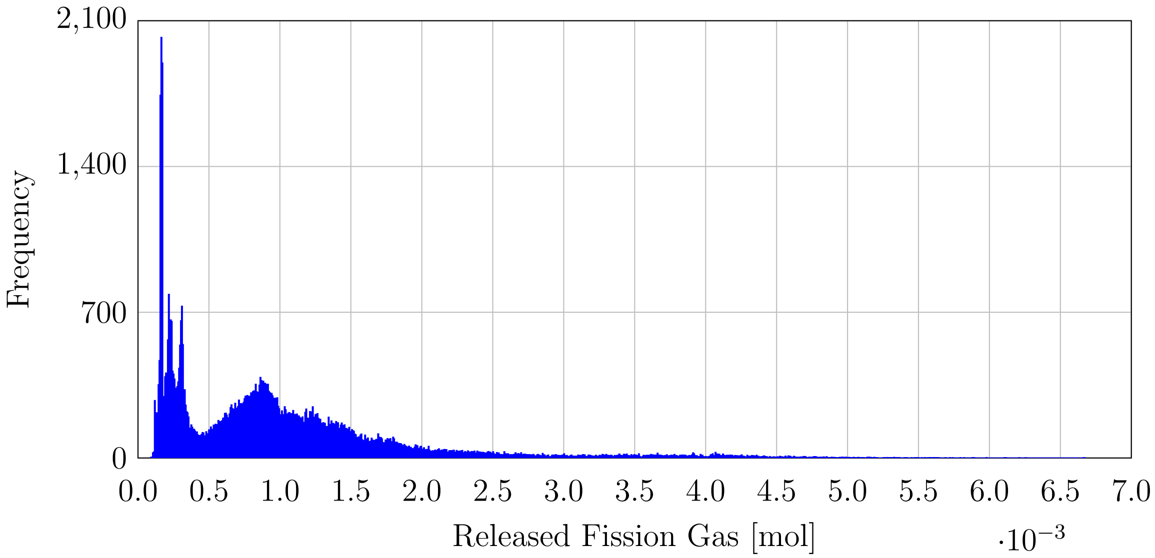

Figure 4.21. The distribution of released fission gas predictions for cycle 1 through cycle 10 fuel rods of WBN1.

4.5 IFBA Layer Helium Production

The helium produced from an IFBA layer is an important consideration when quantifying the discharge RIP of fuel rods with IFBA layers. The amount of helium released from each IFBA layer is calculated from equation 2.30, by utilizing FRAPCON parameters that have been quantified for each WBN1 IFBA rod from representative Polaris cases. The predicted values of the B-10 utilization (β) for every cycle 1 through 10 IFBA rod of WBN1 are shown in Figure 4.22 with respect to the fuel rod discharge burnup. Figure 4.22 reveals that after a fuel burnup of 30 GWd/MTU, over 99% of the initial B-10 has been converted into gaseous helium. Consequently, an assumption with minimal error for IFBA fuel rods with fuel burnups over 30 GWd/MTU is that 100% of initial B-10 loaded into the IFBA layer is converted into gaseous helium. At burnups lower than 30 GWd/MTU, the B-10 utilization can be predicted by equation 2.31. The two curves of Figure 4.22 are due to the spectral differences between the IFBA rods. Explicitly, differences between all of the values in the exponent of equation 2.31, with the exception of the fuel burnup, are the cause of the two curves in Figure 4.22 and are due to differences in the fuel enrichment and specific power of the IFBA rods. The distributions of the predicted B-10 utilization of all cycle 1 through 10 IFBA rods of WBN1 are shown in Figure 4.23. The minimum and maximum predictions for β are 0.9103 and 0.9999, respectively.

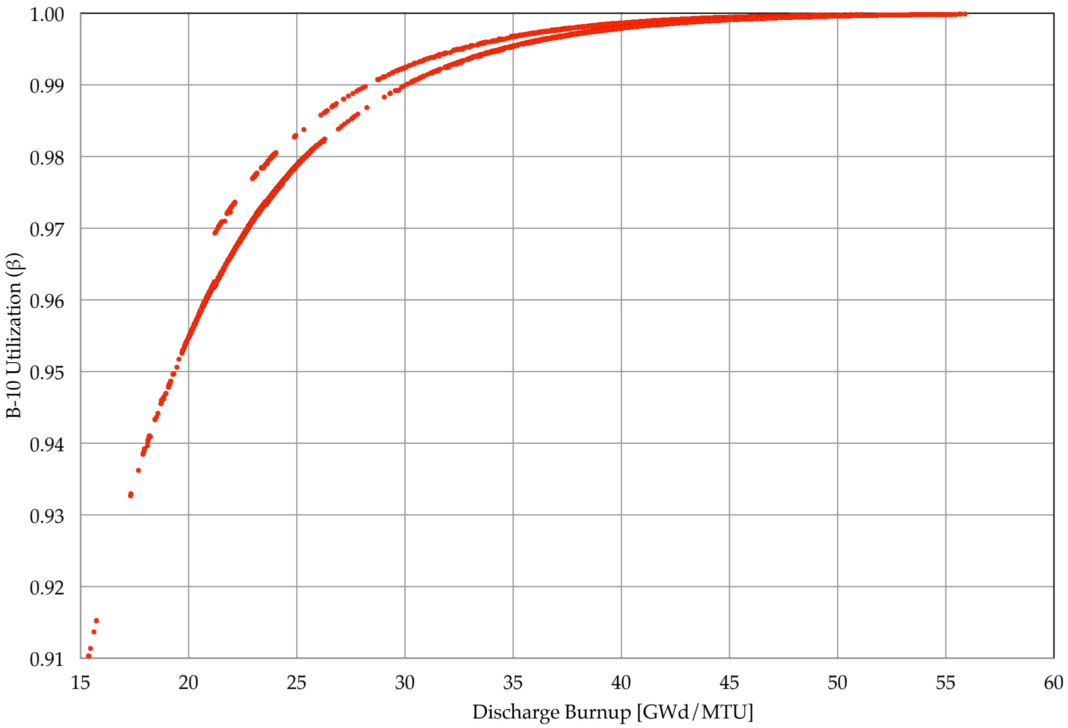

Figure 4.22. The B-10 utilization factor of each ZrB_2 IFBA layer vs. discharge burnup for cycle 1 through cycle 10 fuel rods of WBN1, calculated using equation 2.31.

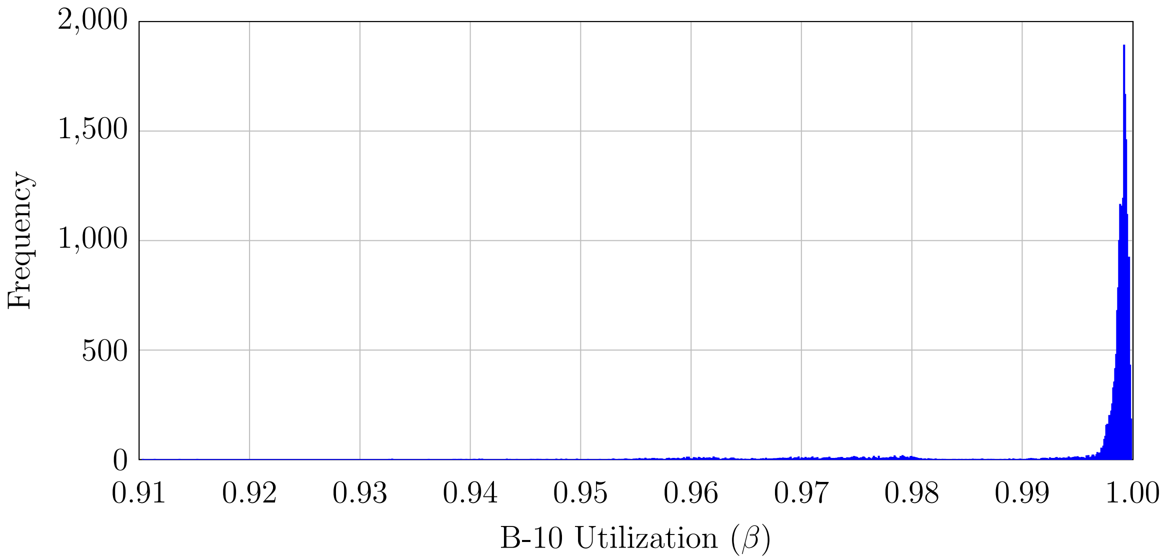

Figure 4.23. The distribution of helium released from ZrB_2 IFBA layers for cycle 1 through cycle 10 IFBA rods of WBN1, calculated from Polaris output data using equation 2.31.

4.6 Rod Internal Pressure

The predicted values for the RIP are shown in Figure 4.24 for both IFBA and standard rods (i.e., fuel rods that do not contain IFBA layers) with respect to their discharge burnups with the density of data shown in Figure 4.25. It is clear from the RIP predictions shown in Figure 4.24 and Figure 4.25 that the presence of an IFBA layer greatly increases the discharge RIP, even while considering reduced fill pressures and annular fuel blankets. The group of data with the highest RIP predictions corresponds to IFBA rods from a single cycle of WBN1, which utilize a reduced fill pressure but do not have annular fuel blankets. Consequently, these rods display the importance of annular blankets in fuel rods with ZrB_2 IFBA layers. RIP predictions for standard rods are bound between about 6 and 8 MPa at vacuum drying conditions across a wide range of discharge fuel burnups. IFBA rods have a larger range of RIP predictions, between 10.5 and 14 MPa when the IFBA rods without annular blankets are excluded. This is due variations in the amount of B-10 loaded onto IFBA rods, which after 30 GWd/MTU is virtually all converted into gaseous helium. The distribution of discharge RIP predictions over 1,000 bins is shown in Figure 4.26. In Figure 4.26, it can be seen that standard fuel rods have RIP predictions of about 6.6 MPa while IFBA rods most commonly have RIP predictions of 11.7 MPa. The minimum and maximum predictions for the RIP are 5.84 and 16.92 MPa, respectively.

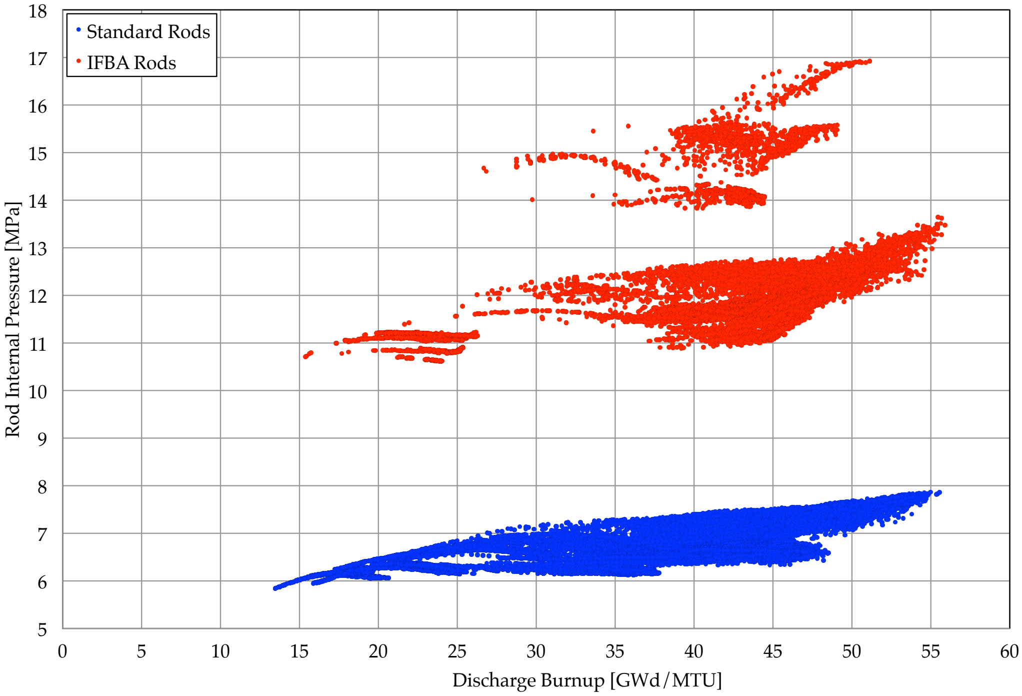

Figure 4.24. Rod internal pressure predictions for cycle 1 through cycle 10 fuel rods under vacuum drying conditions (P_{Ext}=133 Pa, T_F=400°C).

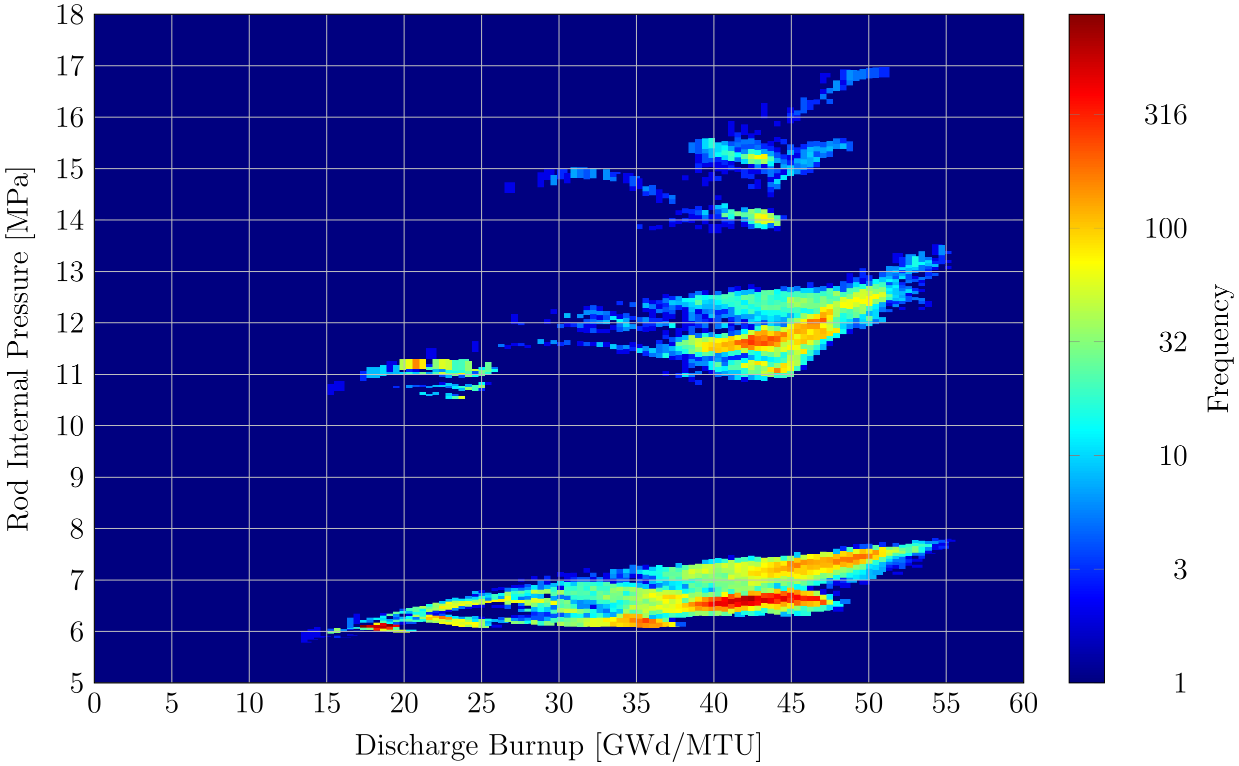

Figure 4.25. Rod internal pressure predictions for cycle 1 through cycle 10 fuel rods under vacuum drying conditions (P_{Ext}=133 Pa, T_F=400°C). Colors correspond to the amount of data within each discharge burnup and RIP bin.

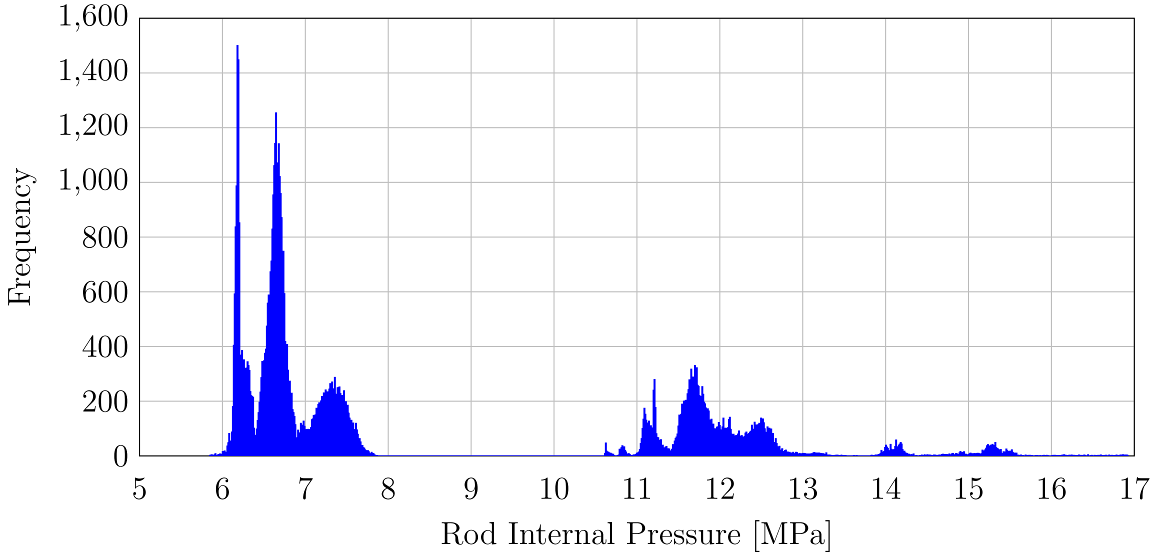

Figure 4.26. The distribution of rod internal pressures for cycle 1 through cycle 10 fuel rods under vacuum drying conditions (P_{Ext}=133 Pa, T_F=400°C).

4.7 Cladding Hoop Stress

If it is assumed that the discharge CHS (σ) has a linear relationship with the RIP (P), a cladding hoop stress factor (F_{CHS}) can be quantified as

$$F_{CHS} = \frac{\sigma}{P}. \tag{4.5}$$

The density and distribution of calculated F_{CHS} values are shown in Figure 4.27 and Figure 4.28, respectively. As is shown in Figure 4.27, the calculated value of F_{CHS} increases with fuel burnup. This is reasonable since as the fuel is irradiated, the oxide thickness present on the fuel cladding surface increases, which increases the CHS predicted by FRAPCON. This is supported by the minor peak shown in Figure 4.28 and the density of data between 15 and 20 GWd/MTU shown in Figure 4.27, which correspond to SNF that was discharged after a single irradiation cycle. It can also be determined that a conservative approximation for F_{CHS} is 7.65, which is greater than virtually all calculated values for WBN1 cycle 1 through cycle 10 fuel rods. The minimum and maximum predictions for F_{CHS} are 7.357 and 7.655, respectively.

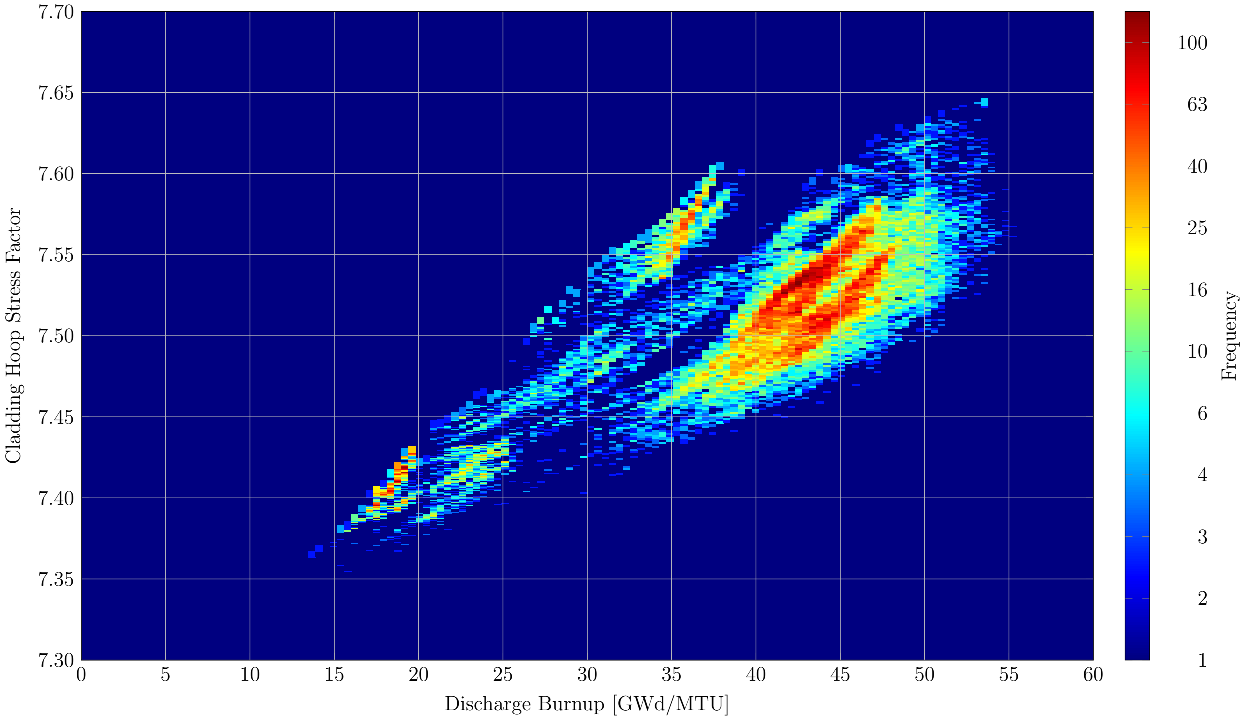

Figure 4.27. Cladding hoop stress factor predictions for cycle 1 through cycle 10 fuel rods under vacuum drying conditions (P_{Ext}=133 Pa, T_F=400°C). Colors correspond to the amount of data within each discharge burnup and cladding hoop stress factor bin.

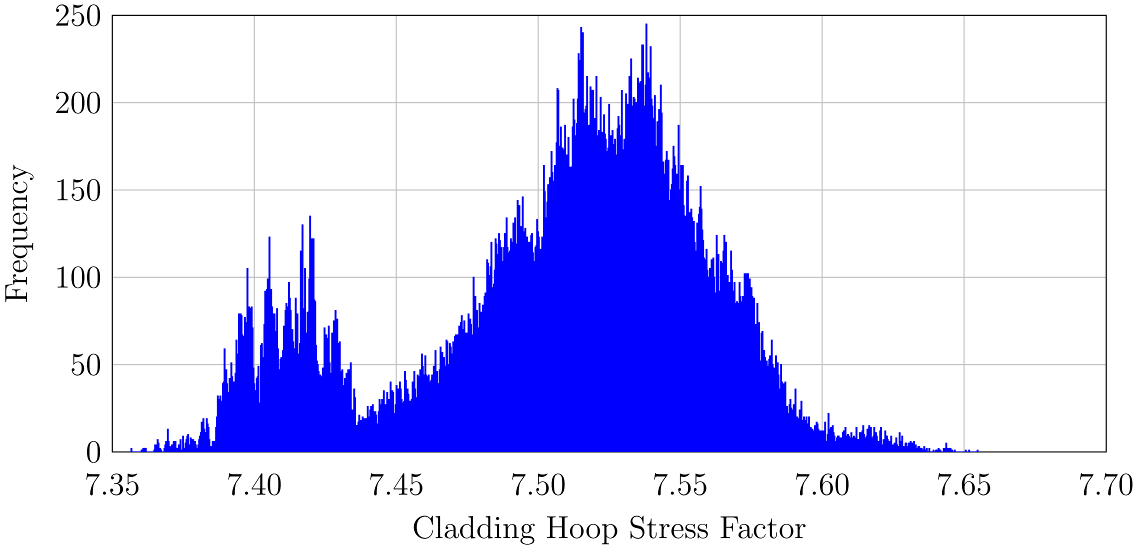

Figure 4.28. The distribution of cladding hoop stress factor predictions for cycle 1 through cycle 10 fuel rods under vacuum drying conditions (P_{Ext}=133 Pa, T_F=400°C).

The value of F_{CHS}, calculated directly from FRAPCON output quantities, provides a means of approximating the CHS for IFBA rods, whose RIP values have been approximated by the post-processing method described previously. Explicitly, once the FRAPCON-predicted RIP of an IFBA rod has been augmented to consider the amount of He released from a ZrB_2 IFBA layer, the CHS of an IFBA rod (σ_{IFBA}) can be approximated by

$$\sigma_{IFBA} = F_{CHS} P_{IFBA}, \tag{4.6}$$

where P_{IFBA} is the predicted RIP of the IFBA rod after post-processing. The CHS predictions for standard and IFBA rods of WBN1 cycle 1 through cycle 10 are shown in Figure 4.29 with the density of data shown in Figure 4.30. The distribution of CHS predictions for cycle 1 through cycle 10 WBN1 fuel rods is shown in Figure 4.31 as a histogram over 1,000 CHS bins. From the data shown in Figure 4.30 and Figure 4.31, CHS predictions for standard and IFBA rods are centered around 50 MPa and 90 MPa, respectively. Similar to the variations observed in the RIP predictions, the variations in CHS predictions of IFBA rods are due to variations in the amount of B-10 present in the IFBA layer. Further, the highest CHS predictions correspond to IFBA rods that do not consider annular fuel blankets. The minimum and maximum predictions for the CHS are 43.02 and 128.11 MPa, respectively.

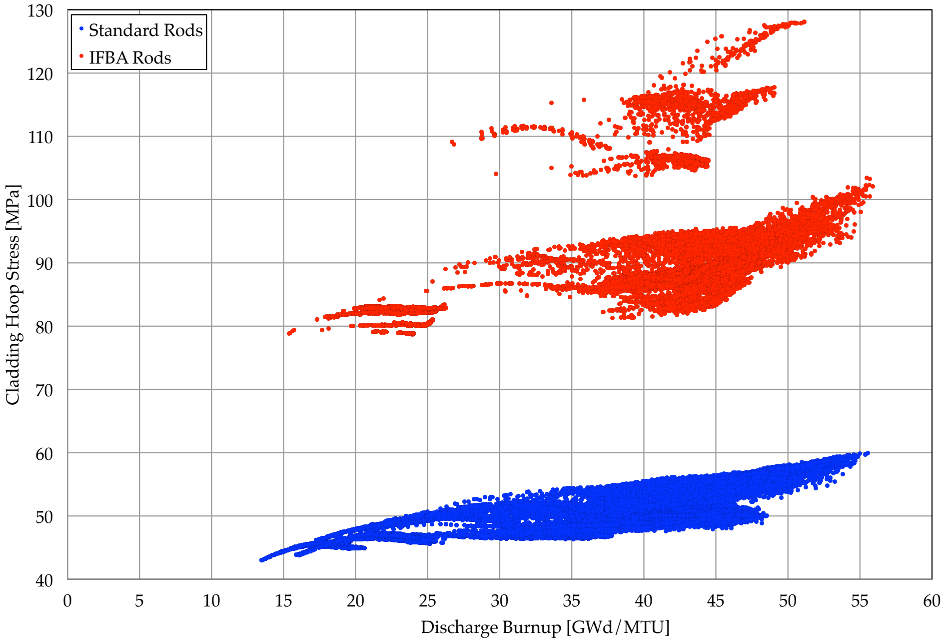

Figure 4.29. Cladding hoop stress predictions for cycle 1 through cycle 10 fuel rods under vacuum drying conditions (P_{Ext}=133 Pa, T_F=400°C).

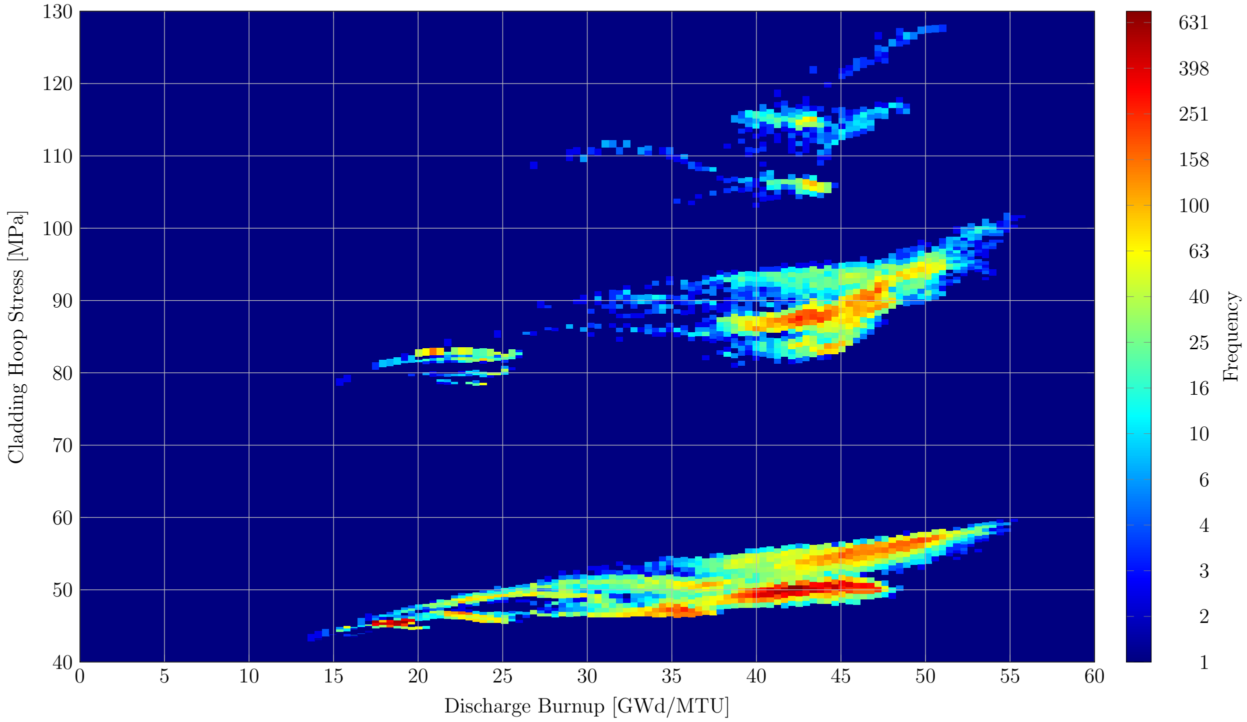

Figure 4.30. Cladding hoop stress predictions for cycle 1 through cycle 10 fuel rods under vacuum drying conditions (P_{Ext}=133 Pa, T_F=400°C). Colors correspond to the amount of data within each discharge burnup and cladding hoop stress bin.

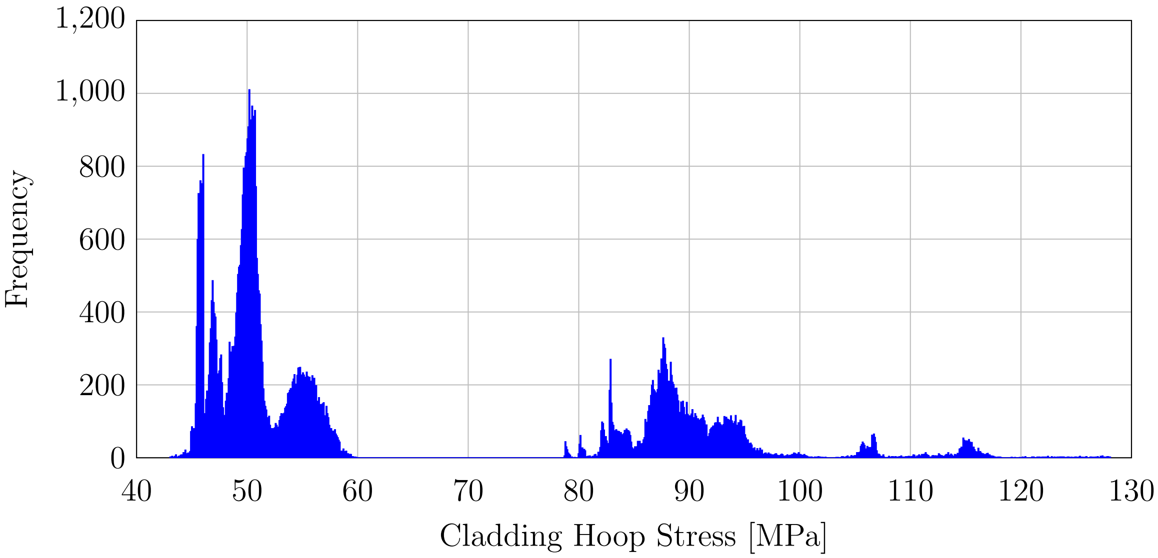

Figure 4.31. The distribution of cladding hoop stress predictions for cycle 1 through cycle 10 fuel rods at vacuum drying conditions (P_{Ext}=133 Pa, T_F=400°C).

5. ANALYSIS

It can be seen in Figure 4.24 that the highest RIP predictions correspond to fuel rods with IFBA layers. The RIP increase due to the introduction of an IFBA layer far exceeds the RIP increase that is observed in Figure 4.24 with an increasing fuel burnup. Specifically, the RIP difference between high- and low-burnup standard rods is about 2 MPa, while the RIP difference between standard and IFBA rods with similar discharge burnups can be up to 9 MPa. Due to the differences in RIP between IFBA and standard rods, the two fuel rod groups will be analyzed separately so that the variables that influence RIP in SNF can be analyzed.

Excluding the system temperature, the final fuel rod void volume and the amount of void gas (henceforth referred to as simply the void volume and void gas, respectively) are the two variables that produce the differences in SNF RIP predictions. If fuel rods with identical IFBA layer compositions, fill gas amounts, and burnups are compared, then the differences in the total void gas are going to be due to differences in the amount of released fission gas. It has been shown in Figure 4.17 and Figure 4.19 that the discharge void volume and the amount of released fission gas depend on the discharge fuel burnup but the behavior of the two parameters with increasing burnup are dissimilar. The amount of fission gas strictly increases with increasing fuel burnup, which is an expected behavior of the FGR models utilized in FRAPCON. Consequently, if only changes in the void gas are considered, the RIP will increase with increasing fuel burnup. The behavior of the void volume with respect to discharge burnup is more complex. Specifically, the final void volume decreases with increasing burnup at burnups less than 30 GWd/MTU and increases with increasing discharge burnups when above 30 GWd/MTU. This can likely be attributed to additional fuel cracking in the fuel, which is expected to increase with increasing fuel burnup, and the thermal expansion of the plenum region of the fuel rod. Variations to both of these volume terms are modeled in FRAPCON throughout the irradiation of the fuel rod and contribute to the total fuel rod void volume [9]. The void volume therefore initially contributes towards an increase in the RIP but, at fuel burnups greater than 30 GWd/MTU, the void volume contributes towards a decrease in the RIP with increasing burnup. The combined contributions of the void volume and void gas towards the discharge RIP can be observed in Figure 4.24 where i) at burnups less than 30 GWd/MTU, the RIP increases with fuel burnup primarily due to the decrease in void volume since the fission gas has increased only slightly at these burnups and ii) at fuel burnups greater than 30 GWd/MTU, the RIP increases due to the increased fission gas since the void volume is beginning to increase. This analysis implies that elevated RIP predictions of SNF (when comparing fuel rods with identical IFBA layers and fill pressures) at burnups greater than 30 GWd/MTU are due to the amount of fission gas present in the fuel rod and not due to the discharge void volume. Of course, any V_f/V_i value less than unity will contribute to an increase in RIP but its upward trend at high burnups implies that its contribution is decreasing.

The RIP at time of discharge (P_f) can be determined from the initial (or fill) conditions and the discharge conditions of the fuel rod by utilizing the following expression

$$P_f = P_i \frac{V_i}{V_f} \frac{n_f}{n_i} \frac{T_f}{T_i}, \tag{5.1}$$

where P_i is the fill pressure of the fuel rod, V, n, and T is the fuel rod void volume, the total amount of gas in the fuel rod void volume, and the fill gas temperature, where the subscripts i and f correspond to the initial and final states of the fuel rod, respectively.

From the data shown in Figure 4.17, an approximation can be made for V_i/V_f for a SNF rod at a specified fuel burnup. For instance, a conservative approximation for V_i/V_f for all WBN1 fuel rods with discharge burnups greater than 45 GWd/MTU is 1.67 (minimum V_f/V_i is 0.60). It should be noted that approximating V_f/V_i from the data shown in Figure 4.17 and Figure 4.18 should only be performed for a fuel rod geometry that is closely related to that of Westinghouse 17x17 assemblies. Since T_f/T_i and P_i will be known quantities and V_i/V_f can be assumed from the data shown in Figure 4.17 and Figure 4.18, the only parameter than needs to be quantified to approximate the discharge RIP using equation 5.1 is n_f/n_i, which can be written in terms of the amount of fill gas (n_{Fill}), the amount of released fission gas (n_{FGR}), and the amount of helium released from an IFBA layer (n_{He}):

$$\frac{n_f}{n_i} = \frac{n_{Fill} + n_{FGR} + n_{He}}{n_{Fill}} = 1 + \frac{n_{FGR} + n_{He}}{n_{Fill}}. \tag{5.2}$$

Further, since n_{FIll} will often be a known quantity and n_{He} can be reasonably quantified from an IFBA helium release model (such as equation 2.30), the only parameter that needs to be quantified for a RIP approximation is n_{FGR}. An additional simplification may be made by assuming that n_{He} is equal to the initial amount of B-10 present in the IFBA layer after a rod-averaged burnup of 30 GWd/MTU, which is supported by the data shown in Figure 4.22. The accurate quantification of n_{FGR} is challenging during fuel depletion simulations and modeling due to the dependence of n_{FGR} on the localized fuel temperature and burnup. Indeed, the axial variations in fuel temperature and burnup must be modeled since the rate of fission gas release from a central pellet may be significantly greater than that of a peripheral pellet, which is still in the athermal region of FGR behavior. If a single fuel-averaged temperature were considered in the quantification of n_{FGR}, the entire duel rod might be considered in this athermal region, while in reality, some central fuel pellets might be in the burst release region of FGR, which would result in an underprediction of n_{FGR}. If n_{FGR} is quantified while considering axial variations in the fuel burnup and temperature (as is done in FRAPCON), then it will provide a reasonable approximation for the discharge RIP if a value for V_i/V_f is assumed.

As specified, the RIP and CHS results produced for the current work consider vacuum drying conditions as the final, or measurement, conditions of the fuel RIP and CHS. If another measurement temperature were desired, the results shown could be recalculated to consider any specified temperature. The rod internal pressure at a second state (P_2) can be written in terms of the RIP and total void volume data reported in the current work (P_1 and V_1, respectively):

$$P_2 = P_1 \frac{V_1}{V_2}\frac{T_2}{T_1}, \tag{5.3}$$

where T_1 corresponds to 673.15 K (or 400°C) and T_2 is the desired rod-averaged plenum gas temperature. The volume at the newly specified temperature (V_2) may need to be determined if there is significant thermal expansion (or retraction) of the cladding and fuel materials between the two temperatures (i.e., V_1/V_2 may not be equal to unity).

With the data provided in Figure 4.24 it is possible to construct a cumulative distribution function (CDF) for IFBA and standard rods with respect to the discharge RIP. CDFs are constructed by integrating the distribution of RIP and CHS predictions shown in Figures 4.26 and 4.31, respectively and normalizing them with respect to the total number of standard or IFBA rods. The CDF for the standard and IFBA rods from cycle 1 through 10 of WBN1 at fuel temperatures ranging from 300 to 400°C are shown in Figure 5.1 and Figure 5.2, respectively. The CDF curves for all plenum temperatures besides 400°C are calculated by utilizing equation 5.3 and the assumption that V_1/V_2 is equal to unity. Figure 5.1 and Figure 5.2 allow for the quantification of the portion of SNF rods that would exceed a defined RIP limit during vacuum drying conditions over a range of rod-averaged plenum gas temperatures across all fuel rod compositions and geometries. For example, if the RIP limit for standard rods is determined to be 7.5 MPa, then the data shown in Figure 5.1 imply that about 5% of the standard rods at 400°C would exceed this limit. Given the data provided in Figure 5.2, a 7.5 MPa limit would be exceeded by all IFBA rods. Another RIP limit may imply that all standard rods are under the designated RIP threshold while some IFBA rods exceed the limit. For instance, if the RIP limit during vacuum drying were set as the system pressure for a typical PWR (2250 psi or 15.5 MPa), then all standard rods would be under this limit while about 1.3% of IFBA rods would exceed this limit at 400°C. A similar analysis can be performed for the discharge CHS of the standard and IFBA rods, the CDFs of which are shown in Figure 5.3 and Figure 5.4, respectively.

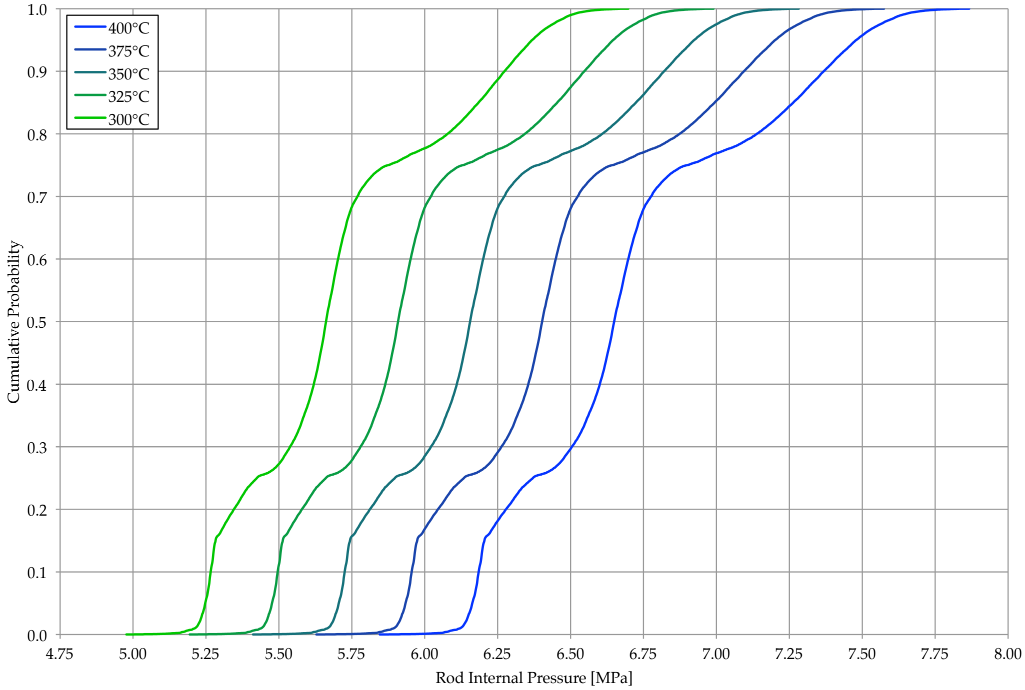

Figure 5.1. The rod internal pressure cumulative distribution function for cycle 1 through cycle 10 standard rods under vacuum drying conditions at various rod-averaged plenum gas temperatures.

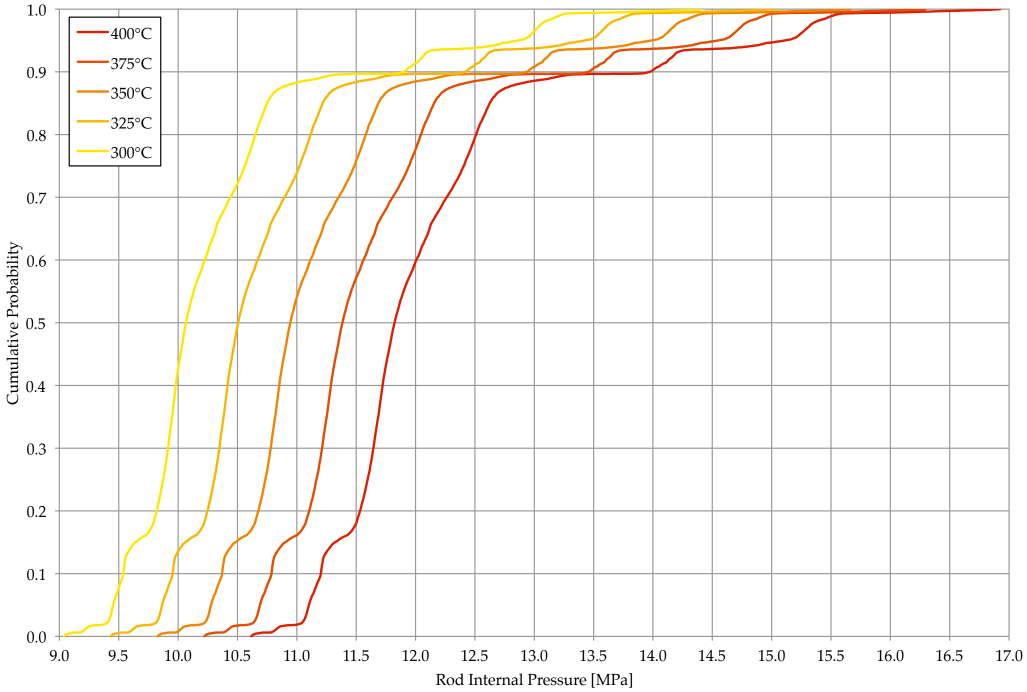

Figure 5.2. The rod internal pressure cumulative distribution function for cycle 1 through cycle 10 IFBA rods under vacuum drying conditions at various rod-averaged plenum gas temperatures.

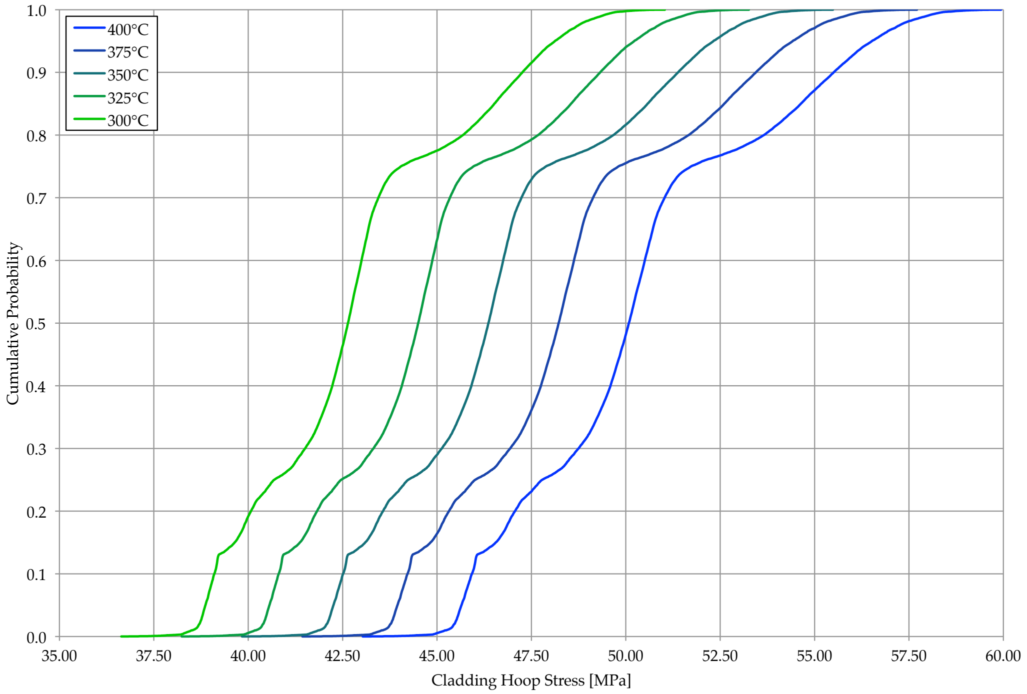

Figure 5.3. The cladding hoop stress cumulative distribution function for cycle 1 through cycle 10 standard rods under vacuum drying conditions at various rod-averaged plenum gas temperatures.

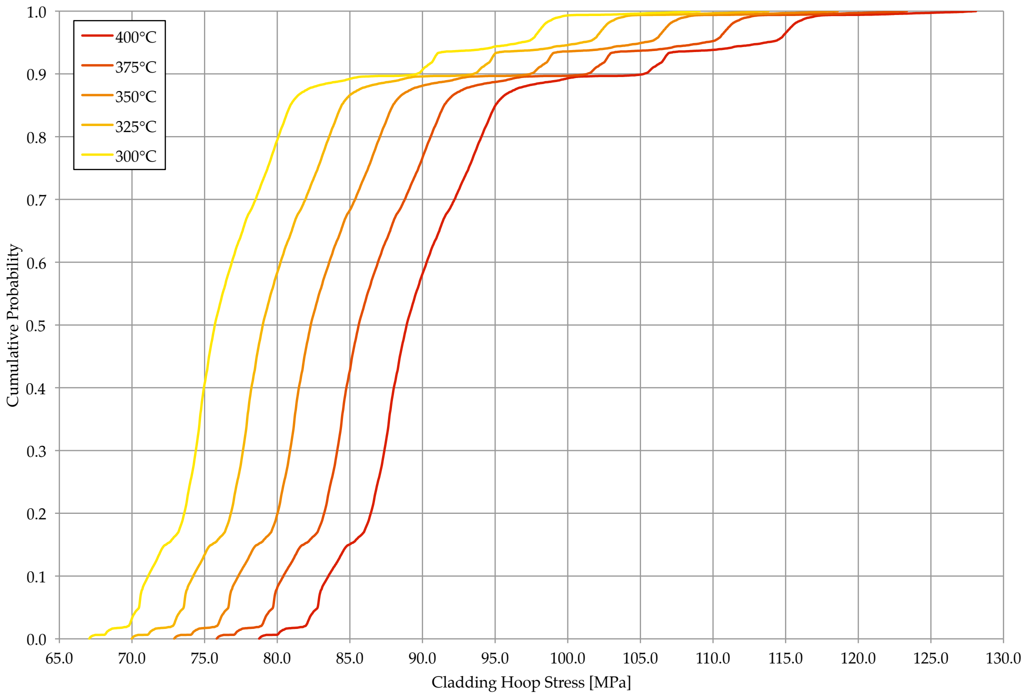

Figure 5.4. The cladding hoop stress cumulative distribution function for cycle 1 through cycle 10 IFBA rods under vacuum drying conditions at various rod-averaged plenum gas temperatures.

It warrants mentioning that the rod-averaged temperatures of fuel rods during the vacuum drying process are not radially uniform across a DSC. In actuality, a radial temperature profile exists across the DSC where fuel rods near the center have a higher rod-averaged plenum temperature relative to fuel rods near the periphery of the DSC. Such a temperature profile is not considered in the current work but if it is assumed that all fuel rods in the DSC have a rod-averaged plenum gas temperature less than 400°C, then the results shown herein represent bounding RIP and CHS predictions. Quantifying the actual distributions of RIP and CHS across a DSC requires knowledge of the radial temperature profile and the loading information of the DSC, which were not available for consideration at the time of the current work.

6. CONCLUSIONS

The current project has quantified the distribution of discharge RIP and CHS predictions for cycle 1 through 10 WBN1 fuel rods at vacuum drying conditions of a DSC. Over 60,000 fuel rods have been modeled in FRAPCON-3.5, taking into account core cycle design data, operation data (including modeling significant trips and downpowers), and as-built fuel enrichments and densities of each fuel rod. A strategy to predict the discharge RIP from a single value (the amount of released fission gas) provided that sufficient data are known regarding the fuel rod fabrication and measurement conditions has been proposed. Cumulative distribution functions have been provided for the RIP and CHS distributions. The results of the current work have been provided in sufficient detail to enable the recalculation of RIP or CHS predictions at any desired thermodynamic state. For example, if the radial temperature profile during vacuum drying and the loading pattern of a DSC were known, then the predicted distributions of RIP and CHS could be calculated for the considered DSC during the vacuum drying process.

The quantitative capabilities of FRAPCON have been utilized and observed extensively, but several changes to the computational methodology of FRAPCON can be proposed based on the challenges encountered during the undertaking of the current project. Based on the RIP predictions shown for WBN1 fuel rods, the proper modeling of the helium released from ZrB_2 IFBA is essential for the proper quantification of RIP and CHS for IFBA rods. Alternatively, for IFBA rods what have been depleted past 30 GWd/MTU, assuming that all of the B-10 has been converted into gaseous helium is expected to introduce minimal error on RIP quantification compared to explicitly quantifying B-10 utilization via equation 2.31. The current model in FRAPCON-3.5 is not satisfactory since it relies on empirical data and does not consider the irradiation history of the fuel rod or the composition of the IFBA layer in sufficient detail. An IFBA model has been derived and proposed in the current work as equation 2.30, which depends on problem-specific parameters such as nuclear data, two-group neutron fluxes, the fuel burnup, and composition of the IFBA layer. Additionally, this model was not derived from nor does it utilize any proprietary data, consequently permitting it for unlimited use and distribution. The proposed IFBA model could be simplified with acceptable error by assuming that all B-10 present in the IFBA is converted into gaseous helium after 30 GWd/MTU (i.e., all high-burnup SNF) and mean or approximate data, that have been quantified in a separate study or in the current work, can be utilized to quantify the exponent in equation 2.30 at all lower fuel burnups. Another proposed improvement to FRAPCON-3.5 is to increase the amount of data that can be used to describe the axial power profile history of a fuel rod or allow the user to specify this value explicitly. In the current work, the axial power profile history of a fuel rod was limited to 20 profiles composed of 53 axial nodes but the fidelity of these computation models would be increased if this limit were relaxed or removed. Modeling the irradiation history of the fuel rod in the highest reasonable fidelity is meaningful since RIP and CHS predictions have been shown to be dependent on local fuel temperatures and burnups through the amount of fission gas released from the fuel. Lastly, the amount of He, Kr, and Xe produced per 100 fissions and the conversion rate between the fast flux and the fuel specific power has been determined to be dependent on the fuel rod irradiation history and fabrication. Consequently, the fidelity of FRAPCON fuel rod models would be increased if the user could provide time-dependent values for these parameters that could be determined from another computational modeling tool, such as SCALE/Polaris. Analyses should be performed to determine the effect that time-dependencies of these parameters would have on RIP and CHS predictions.

Improvements could also be made to the methodology of the current work by utilizing actual manufacturing data for the fuel pellet dishes and chamfers, although this is expected to have a minimal effect on the results since the missing volume due to dishes and chamfers has been conserved in the current work. Further, the irradiation histories of each fuel rod could be modeled such that there is sufficient ramp up and ramp down to consider inter-cycle downtimes in FRAPCON. A more-detailed methodology for quantifying the CHS from a modified RIP should also be developed based on what is utilized in FRAPCON.

REFERENCES

1. (2014) High Burnup Dry Storage Cask Research and Development Project: Final Test Plan, Tech. rep., Electric Power Research Institute.
2. Uffelen, P. V. and M. Suzuki (2012) Comprehensive Nuclear Materials, chap. 3.19, Elsevier Ltd., pp. 535–577.
3. Pastore, G., L. P. Swiler, J. D. Hales, S. R. Novascone, D. M. Perez, B. W. Spencer, L. Luzzi, P. V. Uffelen, and R. L. Williamson (2014) “Uncertainty and sensitivity analysis of fission gas behavior in engineering-scale fuel modeling,” Journal of Nuclear Materials.
4. Machiels, A. (2013) End-of-Life Rod Internal Pressures in Spent Pressurized Water Reactor Fuel, Tech. Rep. 3002001949, Electric Power Research Institute.
5. (2003) Cladding Considerations for the Transportation and Storage of Spent Fuel, Tech. rep., Nuclear Regulatory Commission.
6. Billone, M. C., T. A. Burtseva, and Y. Yan (2012) Ductile-to-Brittle Transition Temperature for High-Burnup Zircaloy-4 and ZIRLO™ Cladding Alloys Exposed to Simulated Drying-Storage Conditions, Tech. rep., Argonne National Laboratory.
7. The HDF Group. Hierarchical Data Format, version 5, 1997-2014. http://www.hdfgroup.org/HDF5/
8. Davis, J. (1999) Volumes, Masses, and Surface Areas for Shippingport LWBR Spent Nuclear Fuel in a DOE SNF Canister, Tech. rep., Oak Ridge National Laboratory.
9. Geelhood, K. J. and W. Luscher (2014) FRAPCON-3.5: A Computer Code for the Calculation of Steady-State, Thermal-Mechanical Behavior of Oxide Fuel Rods for High Burnup, Pacific Northwest National Laboratory, Richland, WA 99352.
10. Berna, G. A., D. D. Lanning, and W. N. Rausch (1981) FRAPCON-2 Developmental Assessment, Tech. rep., Pacific Northwest National Laboratory.
11. Guenther, R. J., D. E. Blahnik, U. P. Jenquin, J. E. Mendel, L. E. Thomas, and C. K. Thornhill (1991) Characterization of Spent Fuel Approved Characterization of Spent Fuel Approved Testing Material - ATM-104, Tech. rep., Pacific Northwest Laboratory.
12. Godfrey, A. T. (2014) VERA Core Physics Benchmark Progression Problem Specifications, Tech. rep., Oak Ridge National Laboratory.
13. (2009) Watts Bar Unit 2 Final Safety Analysis Report (FSAR), Tech. Rep. ML091400651, United States Nuclear Regulatory Commission.
14. Godfrey, A., B. Collins, K. S. Kim, R. lee, J. Powers, B. Salko, S. Stimp- son, W. Wieselquist, R. Montgomery, R. Montgomery, B. Kochunas, D. Jabaay, N. Capps, and J. Secker (2015) VERA Benchmarking Results For Watts Bar Nuclear Plant, Tech. rep., UT-Battelle, LLC, Oak Ridge National Laboratory, http://www.casl.gov/docs/CASL-U-2015-0206-000.pdf.
15. Kang, H. R. (2006) Computational Color Technology, chap. 9, SPIE Publications.